Journal of Marine Research, 45, 871–909, 1987

The freshwater pulse—a numerical model with application to the St. Lawrence Estuary

by Kim-Tai Tee[1] and Thin-Hock Lim[1,2]

ABSTRACT

The freshwater pulse, characterized by a salinity minimum, has been observed in many coastal areas. A 2-D numerical model was developed to investigate the laterally averaged estuarine circulation, and the freshwater pulse in the St. Lawrence Estuary. The effects on the circulation and salinity of various parameters, including vertical eddy coefficients, river runoff, the bottom friction coefficient and the open boundary condition were studied.

The freshwater pulse in the St. Lawrence Estuary was simulated using a seasonal variation of the freshwater runoff. In addition to simulating the downstream propagation and the reduction of the pulse's amplitude toward both the ocean and the deep water in most of the areas, several interesting results were produced. These include (1) the finding of the maximum and minimum amplitudes of the pulse, (2) the increase of the amplitude from surface to deep water in the far upstream region, (3) the initial formation of the pulse at two surface locations, (4) the increase of the arrival time from surface to deep water, and (5) the increase of the arrival time for deep water pulses (at 25 m or deeper) toward the slope region where the upstream shallow water and the downstream deep water separates. The responses of the horizonal and vertical velocities to the freshwater pulse were described. Dynamics associated with the distribution, formation and propagation of the pulse were discussed.

1. Introduction

The freshwater pulse is characterized by a minimum salinity: it originates from spring runoff and ice melting and has been observed in many coastal areas. One such pulse is shown for the Gulf of St. Lawrence area in Figure 1. From the later arrival and smaller amplitude of the pulse downstream (Figs. 1, 2), we can see that it is developed in the St. Lawrence Estuary and then advected to the Gulf. Note that the observed pulses in the Gulf (curves E, F and G) are not originated from local runoff because (1) the runoff has a maximum value in May (Jordan, 1973), much earlier than the arrival of the pulses in July and August, and (2) the magnitude of the local runoff is less than 10% of the runoff through the head of the Estuary. It is important to note that this study only examines the laterally averaged velocity and salinity, and does not involve the cross-channel variation which can be simulated only through a complicated

1. Physical and Chemical Sciences Branch, Department of Fisheries and Oceans, Bedford Institute of Oceanography, Dartmouth, Nova Scotia, Canada, B2Y 4A2.
2. Present address: 993 Ranchview Crescent, Calgary, Alberta, Canada.

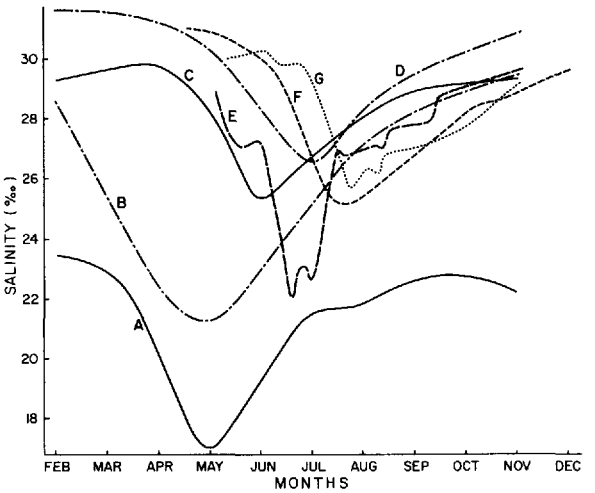

Figure 1. The freshwater pulse in the Gulf of St. Lawrence area. The locations where the data of the curves A, B, C, D, E, F and G were taken are shown in Figure 2 by the corresponding letters. The data on curves B and D are taken to be the average between the north and south shore values. A, C-Neu (1982); B-El-Sabh (1979), D-El-Sabh (1973); E, F, G-Lauzier (1957).

three-dimensional numerical model. An example of the cross-channel variation is the low frequency eddy motion near the Estuary-Gulf boundary, which was found to be significantly correlated with the atmospheric pressure (El-Sabh *et al.*, 1982).

The later arrival and smaller amplitude of the pulse downstream, which is similar to the characteristic of a tracer, is in line with the classical concept that (1) the pulse is developed initially near the head of an estuary, and then advected by a mean current toward downstream locations, and (2) the downstream reduction of the pulse's amplitude is caused by mixing or entrainment of the pulse with deeper or surrounding water. However, because the pulse is characterized by a minimum salinity, and governed by the nonlinear momentum and salt conservation equations, the classical concept of the pulse may not be adequate. The objective of this study is to investigate the distribution, formation and propagation of the freshwater pulse in the St. Lawrence Estuary using a two-dimensional numerical model, and to examine the associated dynamics.

There have been several recent numerical modelling studies of coastal circulation (Blumberg, 1975; Hess, 1976; Leendertse and Liu, 1975; Wang and Kravitz, 1980). They involved a steady or quasi-steady state solution, or a solution that oscillated with a period on the order of days (such as the tidal oscillation). The transient response of a simple estuary (50 km long with constant depth of 20 m) to a sudden increase in freshwater runoff was computed by Wang and Kravitz (1980). In this study, we investigate the response of the St. Lawrence Estuary to the seasonal variation in

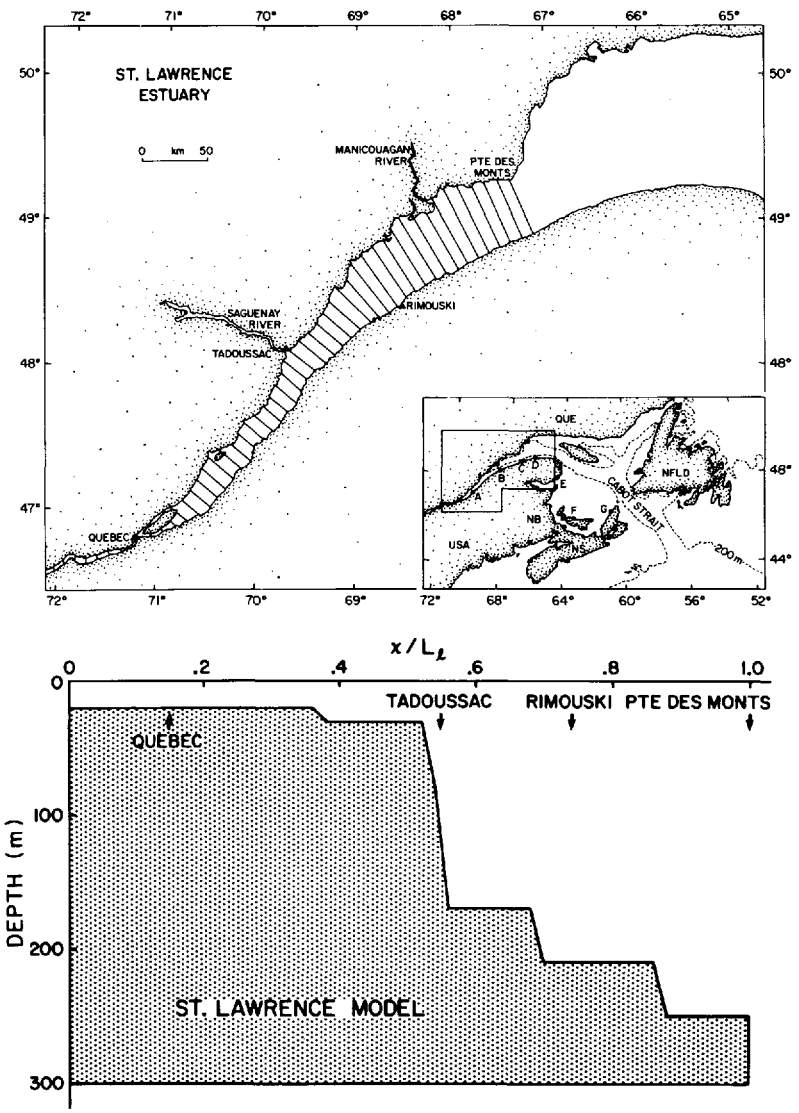

Figure 2. The St. Lawrence Estuary. (a) The location and the numerical grid system of the estuary; (b) the topography of the estuary.

freshwater runoff. The study is interesting scientifically because it is the first that simulates the formation, distribution and propagation of the freshwater pulse in coastal waters.

Two models are considered in this paper: a model of the St. Lawrence Estuary whose topography and the numerical grid system are shown in Figure 2 and a simple model which has a constant cross-section and a topography similar to the St. Lawrence

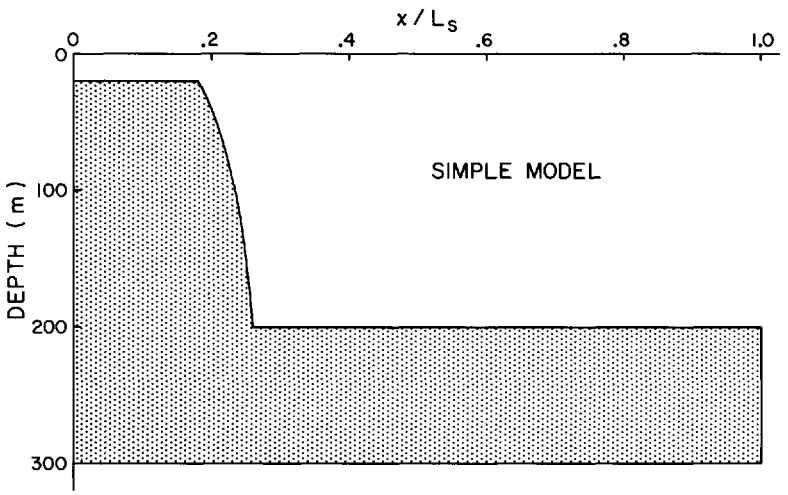

Figure 3. The topography of the simple model.

Estuary (Fig. 3). The simple model is used to examine the sensitivity of the estuary to freshwater runoff, open boundary conditions, and physical parameters such as eddy and frictional coefficients.

The construction of the model is described in Section 2. Some computations for the simple model are given in Section 3. In Section 4, a typical salinity and velocity distribution in the St. Lawrence Estuary is described. Discussions of the amplitude and arrival time of the pulse are given in Section 5. The response of the velocity to the pulse is examined in Section 6.

2. Method of computation

a. Governing equations. The governing equations of the model, averaged over the width of the channel, are:

$$\frac{\partial u}{\partial t} + \frac{1}{B}\frac{\partial (Bu^2)}{\partial x} + \frac{\partial}{\partial z}(uw) = -\frac{1}{\rho_o}\frac{\partial P}{\partial x} + \frac{\partial}{\partial z}\left(N\frac{\partial u}{\partial z}\right) \tag{1}$$

$$\frac{1}{B}\frac{\partial (Bu)}{\partial x} + \frac{\partial w}{\partial z} = 0 \tag{2}$$

$$\frac{\partial s}{\partial t} + \frac{1}{B}\frac{\partial (Bsu)}{\partial x} + \frac{\partial}{\partial z}(sw) = \frac{\partial}{\partial z}\left(K\frac{\partial s}{\partial z}\right) \tag{3}$$

where (1) is the momentum equation, (2) the continuity equation, and (3) the salt conservation equation. The notations in the equations are:

x, z = Cartesian co-ordinates where x is positive seaward from the head of the estuary, and z is positive upward from the surface.

u, w = velocity components in x and z directions,
N, K = coefficients of vertical eddy viscosity and diffusivity,
B = width of the estuary, which is a function of x only,
t = time,
s = salinity,
ρ_o = density of the fresh water, and
P = pressure.

Horizontal diffusion is neglected in this study. In the upper part of the estuary (Neu, 1970; see Fig. 14) where the horizontal diffusion is most significant, the distance (L_x) for 1‰ horizontal variation of salinity is ≈5 km. The value of the horizontal diffusivity (A_h) is very uncertain. In previous modellings of 2-D estuarine circulation (Blumberg, 1975; Hamilton, 1975; Bowden and Hamilton, 1975; Festa and Hansen, 1976; Wang and Kravitz, 1980), A_h varied from 0 to $\approx 10^2$ m^2 s^{-1}. The upper limit of A_h (10^2 m^2 s^{-1}) was found by Blumberg (1975) to be unrealistically high. Using the horizontal velocity scale (u) of 0.1 m s^{-1} (Fig. 8), and the diffusivity scale of 1 to 10^2 m^2 s^{-1}, the ratio of horizontal diffusion to horizontal advection ($A_h/L_x u$) varies from 0.002 to 0.2. Thus, neglecting horizontal diffusion is probably reasonable.

The density (ρ) is related to the salinity by:

$$\rho = \rho_o(1 + \beta s) \tag{4}$$

where β is a constant, numerically equal to 7.57×10^{-4} per ‰. Integrating (2) over the water column, we obtain:

$$\frac{\partial \eta}{\partial t} + \frac{1}{B}\frac{\partial}{\partial x}(D + \eta)BU = 0 \tag{5}$$

where η is the sea level elevation, D is the depth of the water column and U is the depth-averaged value of u. By applying the rigid-lid boundary condition at the surface,

$$w = 0 \text{ at } z = 0$$

the continuity equation (5) can be reduced to:

$$\frac{\partial}{\partial x}(BDU) = 0. \tag{6}$$

The rigid-lid approximation can be applied here because (1) the sea surface elevation (η) is much smaller than the depth of the water column, and (2) the barotropic response time is only a few hours which is negligibly small compared to long period response (on the order of months) considered in this study.

Pressure (P) derived from the hydrostatic approximation is given by:

$$P(z) = P_s + \int_z^o g\rho dz' \tag{7}$$

where P_s is the pressure at rigid-lid surface. By computing the pressure gradient in Eq. (1) from (4) and (7), the momentum equation can be reduced to:

$$\frac{\partial u}{\partial t} + \frac{1}{B}\frac{\partial}{\partial x}(Bu^2) + \frac{\partial}{\partial z}(uw) = -\frac{1}{\rho_o}\frac{\partial P_s}{\partial x} - g\beta\int_z^o \frac{\partial s}{\partial x}dz' + \frac{\partial}{\partial z}\left(N\frac{\partial u}{\partial z}\right). \quad (8)$$

b. Numerical computation. Grid spacing is constant for the x-direction (Δx), and variable in the z-direction (Δz). The velocity component, u, and the salinity, s, are at the same depth, but separated by $1/2\Delta x$.

Given the value of a variable g at adjacent points of x-$\Delta x/2$ and $x + \Delta x/2$, the difference ($\delta_x g$) and average ($\overline{g}^x$) values are defined at the mid-point between them as follows:

$$\delta_x g = \{g(x + 1/2\Delta x) - g(x - 1/2\,\Delta x)\}/\Delta x \quad (9)$$

$$\overline{g}^x = 1/2\{g\,(x + 1/2\,\Delta x) + g(x - 1/2\,\Delta x)\} \quad (10)$$

Similar operators ($\delta_z g, \overline{g}^z, \delta_t g, \overline{g}^t$) are defined with respect to the co-ordinate z and time t. The time step is indicated by the subscript, i.e.,

$$g_n = g(t = n\Delta t). \quad (11)$$

The depth averaged value U can be obtained from (6) as:

$$U = \frac{Q}{BD} \quad (12)$$

where Q is the volume transport of the fresh water at the head of the estuary ($x = 0$). The baroclinic component of u, given by:

$$\tilde{u} = u - U \quad (13)$$

can be solved from (8) using the method developed by Bryan (1969). Let u^* be the solution of u by ignoring the unknown contribution made by the surface pressure P_s that is:

$$\frac{u^* - u}{\Delta t} + \frac{1}{B}\frac{\partial}{\partial x}(Bu^2) + \frac{\partial}{\partial z}(uw) = -g\beta\int_z^o \frac{\partial s}{\partial x}dz + \frac{\partial}{\partial z}\left(N\frac{\partial u}{\partial z}\right) \quad (14)$$

$\tilde{u}$ can be computed from

$$\tilde{u} = u^* - \langle u^*\rangle \quad (15)$$

where $\langle u^*\rangle$ denotes the depth-averaged value of u^*. The completed finite difference form of (14) is:

$$\frac{1}{\Delta t}[u^* - u(t - 1/2\,\Delta t)] + \frac{1}{\overline{B}^x}\delta_x(B\overline{u}^x\overline{u}^x) + \delta_z(\overline{w}^x\overline{u}^z) = -g\beta\sum_{k'=1}^{k}\delta_x\overline{s}^z\,\Delta z_{k'} + \delta_z\,(N\delta_z u) \quad (16)$$

where

$$\sum_{k'=1}^{k}$$

is the summation from level 1 to k, and $\Delta z_{k'}$ is the grid spacing at level k', with $k' = 1$ indicating the first level from the surface. The velocity component u at $(t + 1/2\,\Delta t)$ can be computed from (12), (13) and (15) as

$$u(t + 1/2\,\Delta t) = \frac{Q}{\bar{B}^x D} + u^* - \frac{1}{D}\sum_{k'=1}^{k_z} u^*\,\Delta z_{k'} \tag{17}$$

where k_z corresponds to the maximum number of levels. After obtaining u at the advanced time step, the vertical velocity w can be computed from the continuity equation (2).

Using the computed velocity, the salinity can be computed from (3) which has the following finite difference form:

$$\delta_t s + \frac{1}{B}\delta_x(\bar{B}^x \bar{s}^x u) + \delta_z(w\bar{s}^z) = \delta_z(k\delta_z s). \tag{18}$$

The advective terms in (16) and (18) and the pressure term in (16) are computed in a central time step (leapfrog method), whereas the diffusive terms are computed in a forward time step. Given the initial values of u and s at the first two time steps, (16), (17) and (18) can be iterated to obtain u, w and s at a later time step. The numerical formulation of the governing equation, which is similar to Bryan's three dimensional ocean circulation model, has been shown to conserve energy, mass and salt (Bryan, 1969; Semtner, 1974).

c. Boundary conditions. The boundary conditions at the surface and the bottom are:

$$\left.\begin{aligned} w &= 0 \text{ (rigid} - \text{lid condition)} \\ \frac{\partial u}{\partial z} &= 0 \text{ (no wind stress)} \\ \frac{\partial s}{\partial z} &= 0 \text{ (no salt flux)} \end{aligned}\right\} \text{for all } x \text{ and } t \text{ at } z = 0 \tag{19}$$

$$\left.\begin{aligned} u_n &= 0 \text{ (zero normal velocity)} \\ N\partial u/\partial z &= \lambda u_b \text{ (bottom friction)} \\ \partial s/\partial z &= 0 \text{ (no salt flux)} \end{aligned}\right\} \text{for all } x \text{ and } t \text{ at } z = -D \tag{20}$$

where u_n is the normal velocity at the bottom, u_b is the horizontal velocity near the bottom, and λ is the linear friction coefficient which is approximated by KU_T where K is 0.0025, and U_T is the magnitude of the tidal current. At the solid boundary, normal velocity and salt flux are both zero.

At the head of the estuary ($x = 0$), we specify the volume transport of the river runoff (Q), and set $s = 0$ (fresh water) at all depths. As in the study of Festa and Hensen (1976), we apply a parabolic velocity profile at the head of the estuary, which can be written as:

$$u = \frac{Q}{BD}\left\{1 + \frac{(1/2)\lambda D}{3N + \lambda D} - \frac{(3/2\lambda D)}{3N + \lambda D}\left(\frac{z}{D}\right)^2\right\}. \tag{21}$$

This profile of u satisfies the conditions $\partial u/\partial z = 0$ at the surface, $N\,\partial u/\partial z = \lambda u_b$ at the bottom, and $Q = UBD$ where U is the depth-averaged value of u.

At the open boundary between estuary and ocean, the salinity is specified in the inflow region and extrapolated in the outflow region. The specified salinity at the open boundary is fixed to the observed value (Neu, 1970) in the St. Lawrence model, and to a constant value of 34.9% in the simple model. In the outflow region, three formulae are used to extrapolate the salinity from the interior value:

$$(i)\ \frac{\partial^2 s}{\partial x^2} = 0 \tag{22}$$

$$(ii)\ \frac{\partial s}{\partial t} + c\frac{\partial s}{\partial x} = 0 \tag{23}$$

$$(iii)\ \frac{\partial s}{\partial t} + u\frac{\partial s}{\partial x} + \frac{us}{B}\left(\frac{\partial B}{\partial x}\right) = \frac{\partial}{\partial z}K\frac{\partial s}{\partial z}. \tag{24}$$

The phase speed c in the Sommerfield radiation condition (23) is taken to be the velocity at the boundary point. The phase speed has also been calculated by using the formula developed by Orlanski (1976). This calculation does not produce any better solutions than those using other formulae. The third formula is derived by assuming that vertical advection at the open boundary is insignificant, which is reasonable near the surface for the well-established estuary (far away from the salt-wedge region near the head of the estuary) in the downstream location (Pritchard, 1954, 1956). The salinity gradient in (24) is obtained by either using backward differencing, or by computing s at half-grid spacing inside the open boundary, and then extrapolating to obtain s at the boundary. For the numerical computation described in the next section, these two methods of obtaining the salinity gradient produce more or less identical solutions. The open boundary condition is discussed further in Section (3a).

The extrapolation of the velocity at the open boundary is required only when the nonlinear advective terms are included in the momentum equation. Two methods are used to compute the advective terms at the open boundary: the first is to set u (outside estuary) = u (at open boundary) and $w = 0$ outside the boundary, and the second is to set the advective terms at the boundary equal to those at half grid spacing inside the boundary. For the following computation, it is found that the nonlinear advective terms computed by using the above extrapolations do not contribute significantly to the solution.

The surface pressure term ($\partial P_s/\partial x$) does not pose any problem in the open boundary condition in this study because it is not involved in the computation. Note from Section (2b) that, because of the rigid-lid approximation, the barotropic velocity component U can be easily computed from (12). The computation of the baroclinic velocity component $\tilde{u}$, which is related to the solution of u^* (14, 15), does not include the surface pressure term.

d. Parameters. One of the major problems in coastal modelling is uncertainties about the value and form of the vertical eddy viscosity coefficients. The determination of the exact value and form of this coefficient, which would require accurate experimental data, is not the objective of this paper. Here the vertical eddy coefficients, N and K, are taken to be either constants, or a function of the Richardson number:

$$N = a + b\,(1 + 7R_i)^{-1/4}$$

and

$$K = (1/2)a + b(1 + R_i)^{-7/4} \tag{25}$$

where

$$R_i = g\beta \frac{\partial s}{\partial z} \Big/ \left(\frac{\partial u}{\partial z}\right)^2$$

is the Richardson number, and a and b are constants. These forms of N and K were chosen by Bowden and Hamilton (1975) for their studies of the estuarine circulation. The values of a and b are chosen between 3×10^{-4} m^2 s^{-1} and 5×10^{-4} m^2 s^{-1}. The linear friction coefficient λ varies from 0.001 m s^{-1} to 0.003 m s^{-1}.

The estuary is divided along its length into 49 equal grid spacings Δx. The length of the simple model, L_s, is 1090 km, which is the distance between the head of the estuary and Cabot Strait (Fig. 2), so that $\Delta x \approx 22.2$ km. For the St. Lawrence model (Fig. 2), the length L_l is 466 km so that $\Delta x \approx 9.5$ km. There are 12 levels in the vertical column. The grid spacing Δz between the levels has variable values. For the simple model, the values of Δz, beginning from the surface, are 10 m each for the first seven spacings, 20 m each for the next three spacings, and 30 m and 40 m for the last two spacings. The values of Δz for the St. Lawrence model are 10 m each for the first six spacings, 20 m each for the next two spacings, 30 m for the following spacing and 40 m each for the last three spacings.

The choice of the time step Δt depends on several linear stability criteria. The Courant-Friedrichs-Lewy criterion gives:

$$\Delta t \leq \Delta x / u_{\max} \tag{26}$$

where $u_{\max}$ is the maximum value of u. The above criterion does not apply to the fast moving surface wave because the wave is filtered out in our rigid-lid model. This absence of the surface wave allows us to use a larger Δt and thus makes our computation much more efficient than other estuarine circulation models (i.e., Blumberg, 1975; Hamilton, 1975, Festa and Hansen, 1976). The Courant-Friedrichs-Lewy criterion, although it is not applicable here for the external gravity wave, should

be considered for internal waves. The simple analysis of the internal wave, using the hydrostatic and rigid-lid approximation, gives the phase speed C_I as:

$$C_I = \frac{f_N D}{n\Pi} \tag{27}$$

where

$$f_N = \left(\frac{g}{\rho}\frac{\partial \rho}{\partial z}\right)^{1/2}$$

is the buoyancy frequency and n is the mode number. The Courant-Friedrichs-Lewy criterion is thus:

$$\Delta t < \Delta x \Big/ \left(\frac{f_N D}{\Pi}\right). \tag{28}$$

In the shallow part of the estuary, f_N can be scaled to $(g/\rho\,\Delta\rho/D)^{1/2}$ so that (27) becomes:

$$C_I \approx \sqrt{gD}\left(\frac{1}{n\Pi}\left(\frac{\Delta\rho}{\rho}\right)^{1/2}\right). \tag{29}$$

Thus, the phase velocity of the internal gravity wave is reduced from that of the external gravity wave ($\sqrt{gD}$) by a factor of $(1/n\Pi(\Delta\rho/\rho)^{1/2})$. The maximum time step is then:

$$\Delta t \leq \frac{\Delta x}{\sqrt{gD}} \frac{\Pi}{\left(\left(\frac{\Delta p}{p}\right)^{1/2}\right)}. \tag{30}$$

The diffusion term gives the limitation of Δt *as:*

$$\Delta t \leq \frac{\Delta z^2}{2N}. \tag{31}$$

Another limitation of Δt arises from the numerical formulation of a vertical diffusion near the bottom where the stress is given by $p\lambda u_b$ (20). The finite difference form of the acceleration and diffusion terms near the bottom is:

$$\delta_t u_b = \frac{1}{\Delta z}\left[N\frac{(u(2) - u_b)}{\Delta z} - \lambda u_b\right] \tag{32}$$

where u_b is the velocity at the first grid point from the bottom, and u (2) is the velocity at the next grid point. Note that the right-hand side of (32) is written in the forward

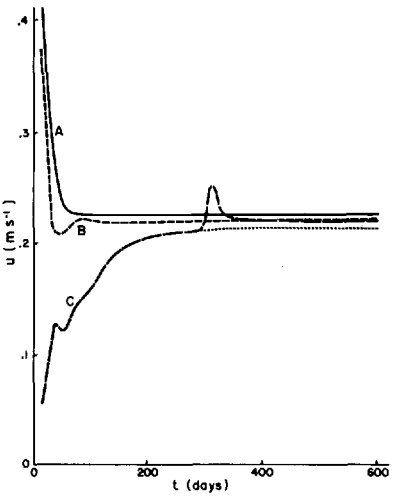

Figure 4. The time variation of the surface velocity u at the middle of the estuary ($x = 0.5\ L_s$), computed in the simple model with (Eq. 25) $a = 10^{-3}\ m^2\ s^{-1}$, $b = 0$ and R (runoff per unit width) $= 0.2\ m^2\ s^{-1}$. The curves A, B and C correspond respectively to the cases of using the boundary conditions (22), (23) and (24).

time step. It can be shown that a linear stability analysis gives the limitation of Δt as:

$$\Delta t \leq \frac{\Delta z}{(N/\Delta z + \lambda/2)}. \tag{33}$$

To examine which of the above criteria impose a lower limit of Δt which can be applied in the numerical computation, we consider the following parameters for the St. Lawrence model: $\Delta x = 9.5$ km, $\Delta z = 10$ m, $\lambda = 3 \times 10^{-3}\ m\ s^{-1}$, $N = 10^{-3}\ m^2\ s^{-1}$, $D = 250$ m, $u_{max} = 1\ m\ s^{-1}$ (near the head), $\partial\rho/\partial z \approx 12‰/40$ m (near the slope region). The values of Δt are 9500 sec limited by the advection (23), 2520 sec by the internal gravity wave (25), 50,000 sec by the diffusion (28) and 6700 sec by the bottom friction (30). Thus, the maximum value of Δt (2520 sec) that can be applied is limited by the internal gravity wave. During the initial spin up computation, the maximum value of Δt is smaller than the above indicated value because of the strong salinity gradient that exists in the vertical column. In the following computation, $\Delta t = 850$ sec and 1700 sec are used respectively for the St. Lawrence model and the simple model.

3. Simple model

a. Initial spin up and open boundary conditions. Figure 4 shows the surface velocity (u) at the middle estuary for the three open boundary formulations (22–24). Other parameters of this computation are $a = 10^{-3}\ m^2\ s^{-1}$, $b = 0$ (no stratification effect on the vertical eddy viscosity), and the freshwater runoff per unit width through the head

of the estuary $R = Q/B = 0.2$ m^2 s^{-1} which may correspond to the typical runoff of 10^4 m^3 s^{-1} for the St. Lawrence Estuary and the typical width of 50 km for the lower estuary (Fig. 2a). Curves A, B and C correspond respectively to the cases of using the boundary conditions (22), (23) and (24). From the figure we can see that the initial response of the system varies very significantly, with u increasing rapidly to over 0.4 m s^{-1} in a very short time for the curves A and B, and smoothly for the curve C. The large values of u for the curves A and B are due to the development of strong currents at the open boundary for these two cases. This result indicates that the boundary condition (24) is probably more reasonable than the other two conditions. In the steady state, Figure 4 shows that the numerical results for the three cases are almost the same. This similarity has also been found for the response of the studied estuary to the slow variation of the freshwater runoff, such as the seasonal variation of the runoff, or the runoff that decreases to half of its value in three days. As the study of the freshwater pulse involves the slow variation of the freshwater runoff (in the order of months), we can see that although the three open boundary formulations influence significantly the initial spin up of the estuary, they do not contribute much uncertainty to the steady state solution, and the solution of the freshwater pulse. In the following computation, Eq. 24 is used.

By changing the freshwater runoff into the system, the salinity in the deep water is expected to vary slightly. By fixing the salinity in the inflow region of the open boundary, we thus introduced a small error in our computation. However, from a series of numerical experiments on both the simple model and the St. Lawrence model, it was found that this error was insignificant because (1) the horizontal advection of the freshwater pulse was negligibly small in the deep water of the open boundary so that the error was not transmitted into the interior region; and (2) near the open boundary, the freshwater pulse in the deep water, which was induced by vertical diffusion of the surface pulse, was very small (see Fig. 16), and was not expected to produce any significant effect near the surface. In the upper outflow portion of the open boundary, any error due to uncertainties of the open boundary condition is advected out of the system, and is not expected to affect significantly the pulse in the upstream region. To confirm that the uncertainties of the open boundary have little effect on the freshwater pulse, we moved the location of the open boundary in the simple model from $x = L_s$ to $x = .6\ L_s$ and found that the response in the interior region remained more or less unchanged.

Another anomalous feature in Figure 4 is the occurrence of a peak at about 320 days on curve C. This peak is caused by changing flow conditions at one grid point of the open boundary. When the flow changes its direction from outflow to inflow at the open boundary, the salinity at the corresponding grid point changes from the value estimated from (24) to 34.9‰. Since this produces a large change of salinity in one time step, it is expected that a disturbance is developed at the open boundary. By locating the peaks on the velocity curve in the horizontal direction, we can see the propagation of the disturbance from the open boundary to the interior region. To

prevent such development of the disturbance at the open boundary, it is found that the salinity at the grid point where the changing of the boundary condition occurs can be specified from the last extrapolated value before the flow reverses its direction. The dashed line in curve C of Figure 4 shows that, by using this new specification of the salinity, the peak at day 320 disappears.

The anomalous disturbance shown in Figure 4 is mainly caused by our specification of constant salinity of 34.9‰ at the inflow part of the open boundary. In practical computations, such as the modelling of St. Lawrence Estuary (Section 4), the disturbance is small because, consistent with the model prediction, the specified salinity at the open boundary increases with depth, so that the difference between the computed and specified salinity at the interface of the open boundary is small. In the following computation, the disturbance is suppressed by setting the salinity at the grid point where the changing from outflow occurs, to the last extrapolated value.

b. Parameter studies. Three parameters are examined in the simple model: the vertical eddy viscosity and diffusivity (N, K); (b) the freshwater runoff (R), and (c) the linear friction coefficient (λ). The difference between this and other parameter studies (Blumberg, 1975, Bowden and Hamilton, 1975; Festa and Hansen, 1976; Wang and Kravitz, 1980) is that, instead of a small and shallow estuary, we consider a long estuary which has a steep slope connecting the shallow channel (20 m) from the deep channel (200 m). The results for the shallow channel are generally consistent with the previous studies. However, as will be shown in the following discussion, some different results from other studies are found for the deep channel.

Figure 5 shows the surface salinity and velocity for three cases of study: (i) $a = 10^{-3}\ m^2\ s^{-1}$, $b = 0$ (constant eddy coefficient, Eq. 5), R (runoff) $= 0.2\ m^2\ s^{-1}$ (curve A); (ii) $a = b = 0.5 \times 10^{-3}\ m^2\ s^{-1}$ (stratification-dependent eddy coefficient), $R = 0.2\ m^2\ s^{-1}$ (curve B); (iii) $a = b = 0.5 \times 10^{-3}\ m^2\ s^{-1}$, $R = 0.4\ m^2\ s^{-1}$ (curve C). By comparing curves A and B, we can see that, as the stratification effect reduces the mixing in the water column, the surface salinity and velocity in the lower estuary decrease. However, because of the larger penetration of the oceanic water to the upstream region, the surface salinity and velocity in the upper estuary increase with the stratification effect.

By doubling the freshwater runoff (compare curves C and B), the salinity becomes smaller, and the velocity becomes larger. The increase in velocity is most significant in the middle part of the estuary. By examining the vertical structure of the velocity, it is found (Fig. 6) that, instead of a two-layer circulation generally predicted for a partially stratified estuary, or in the estuary with smaller runoff ($R = 0.2\ m^2\ s^{-1}$), a small outflow is induced at the deep water (100 m) which splits the inflow near the slope region and creates a small maximum outflow near the mouth of the estuary. By decreasing the linear bottom friction coefficient (λ) from $3 \times 10^{-3}\ m\ s^{-1}$ to $10^{-3}\ m\ s^{-1}$, it is found that the results are more or less the same. In the following discussion, $\lambda = 3 \times 10^{-3}\ m\ s^{-1}$ is used.

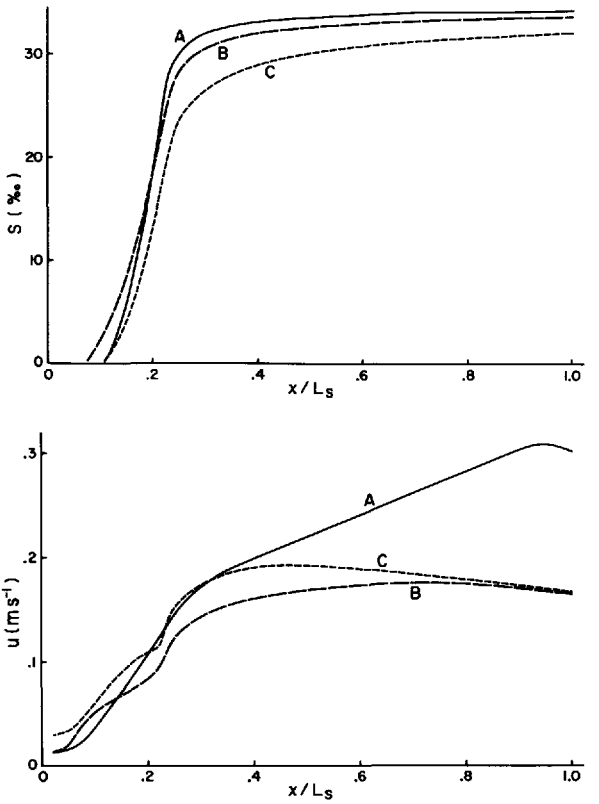

Figure 5. The horizontal variation of the steady state solution of (a) surface salinity s, and (b) surface velocity in the simple model for different values of mixing coefficient (25) and runoff per unit width (R). (A) $a = 10^3\ m^2\ s^{-1}$, $b = 0$, $R = 0.2\ m^2\ s^{-1}$; (B) $a = b = 0.5 \times 10^{-3}\ m^2\ s^{-1}$, $R = 0.2\ m^2\ s^{-1}$; (C) $a = b = 0.5 \times 10^{-3}\ m^2\ s^{-1}$, $R = 0.4\ m^2\ s^{-1}$.

4. Typical salinity and velocity distribution in the St. Lawrence Estuary

There are three major river inputs to the St. Lawrence Estuary: the St. Lawrence River through Quebec City, the Saguenay River near Tadoussac, and the Manicouagan River system near Pointe des Mont (Fig. 2). Averaging the runoff from 1950 to 1976, the minimum winter runoff and the maximum spring runoff are respectively 9860 $m^3\ s^{-1}$ and 16300 $m^3\ s^{-1}$ up to Quebec City, 11300 $m^3\ s^{-1}$ and 19590 $m^3\ s^{-1}$ up to Tadoussac (Saguenay River included), and 12620 $m^3\ s^{-1}$ and 21030 $m^3\ s^{-1}$ up to Pointe des Mont (Saguenay River and Manicouagan River system included) (F. Jordan, Bedford Institute of Oceanography, private communication). Since the freshwater runoff through Quebec City accounts for 78% of the total runoff into the St. Lawrence Estuary, only this runoff from the head of the estuary is included in this study. As the Manicouagan River System is near the open boundary of our model (Fig. 2) and thus unlikely to have a strong influence on the upstream region of the estuary, the input of

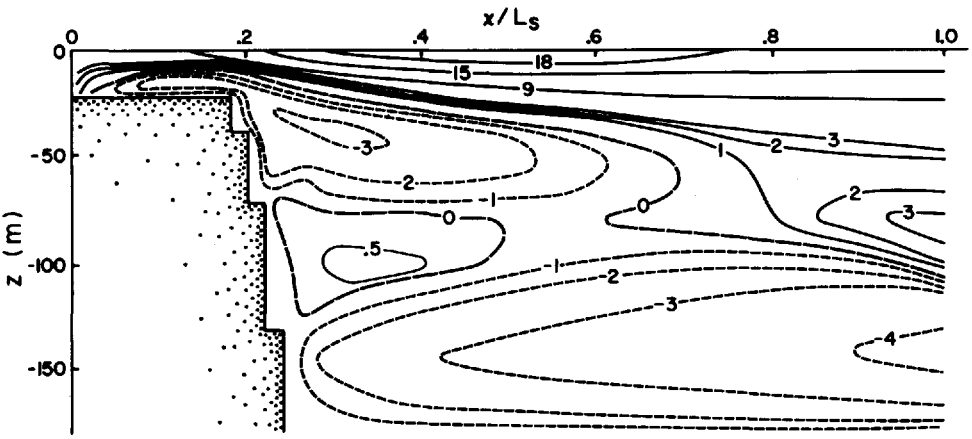

Figure 6. The steady state horizontal velocity u of the simple model wtih (Eq. 25) $a = b = 0.5 \times 10^{-3}$ m^2 s^{-1} and R (runoff per unit width) = 0.4 m^{2}s^{-1}.

the freshwater runoff in this study in fact accounts for about 85% of the input for the region. Figure 7 shows the seasonal variation of the freshwater runoff per unit width (R) averaged between 1950 and 1976 through the head of the estuary (F. Jordan, private communication). The 1963 runoff is also included in the figure. In the following computation, the averaged runoff (solid curve in Fig. 7) is used.

The computed horizontal and vertical velocity, and salinity of the St. Lawrence Estuary at day 140 (mid-May), the typical distribution for all seasons, are shown in

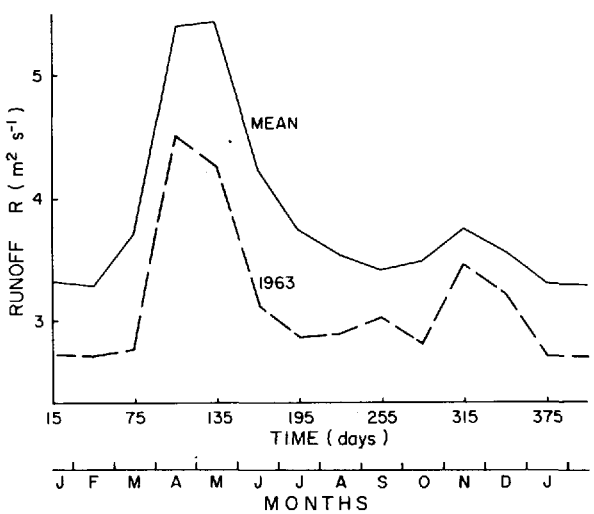

Figure 7. The mean (1950–1976) and 1963 seasonal runoff per unit width (R) in the St. Lawrence Estuary. (F. Jordan, Bedford Institute of Oceanography, private communication).

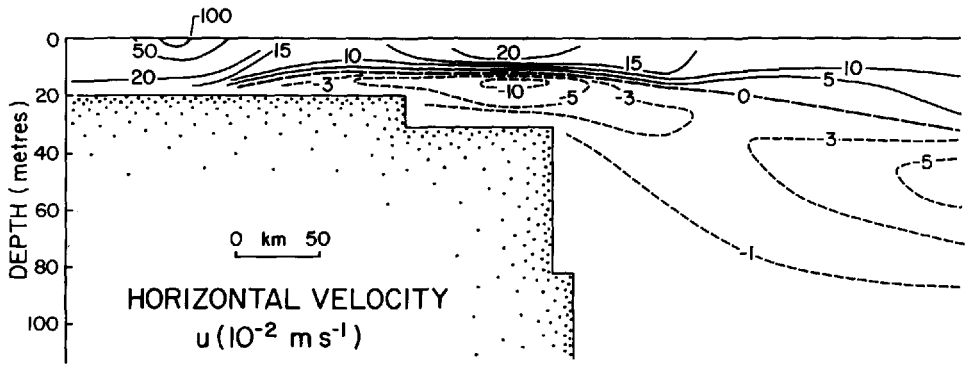

Figure 8. The horizontal velocity u of the St. Lawrence Estuary at the day 140 (mid-May), $a = b = 0.3 \times 10^{-3}\ m^2\ s^{-1}$ (Eq. 25).

Figures 8, 9 and 10. The horizontal velocity shows a two-layer flow with the interface deepening toward the oceanic boundary. Besides the maximum current that occurred near the head of the estuary, there is a second maximum current that occurred near the slope region. The amplitude of the current is generally the same order as the observed value (Forrester, 1967; El-Sabh, 1977). For the vertical velocity, the upwelling occurs near the slope region. The maximum amplitude of the vertical velocity is in the order of $2 \times 10^{-5}\ m\ s^{-1}$. Because of the entrainment of down-estuary flow from the lower layer, it is expected that the vertical velocity is generally in the upward direction. The reason for the maximum vertical velocities near the slope regions is that the up-estuary flow in the lower layer is diverted upward to the surface layer because of blocking by the solid boundary in the slope region.

The salinity shows a smaller horizontal variation downstream of the slope region than that upstream of the slope region, which generally agrees with previous studies (Borne de Grandpre and El-Sabh, 1980; Borne de Grandpre *et al.*, 1981). The velocity

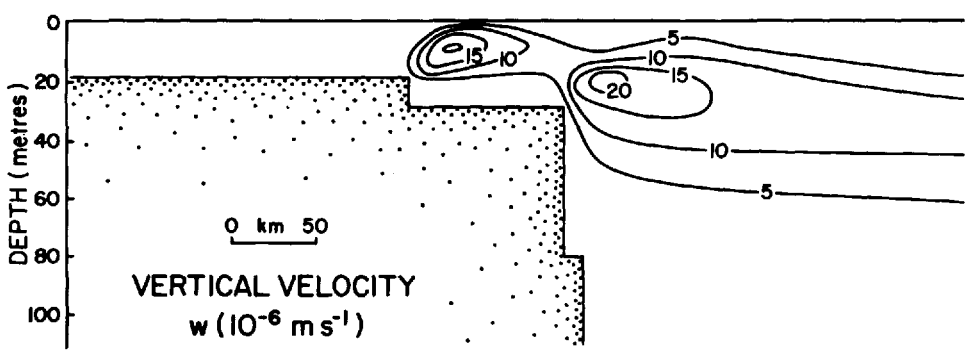

Figure 9. The vertical velocity w of the St. Lawrence Estuary at the day 140 (mid-May). $a = b = 0.3 \times 10^{-3}\ m^2\ s^{-1}$ (Eq. 25).

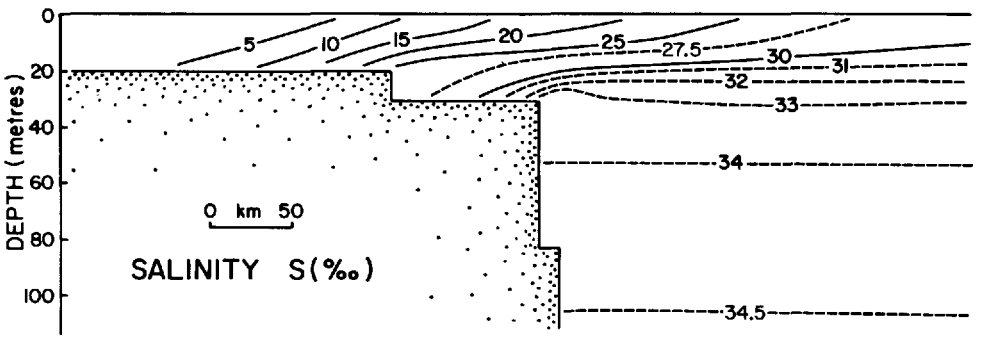

Figure 10. The salinity s of the St. Lawrence Estuary at the day 140 (mid-May). $a = b = 0.3 \times 10^{-3}$ m^2 s^{-1} (Eq. 25).

and salinity in the deep water (below 115 m), because of the negligible salinity gradient and velocities, are not shown in the figure.

To study the dynamics associated with the above typical distribution of velocity and salinity, we examine the balance of terms in the momentum and salinity equations (1, 3). Using (2) and (7), the two equations can be rewritten as

$$\frac{\partial u}{\partial t} + u\frac{\partial u}{\partial x} + w\frac{\partial u}{\partial z} + \frac{1}{\rho_o}\frac{\partial P_s}{\partial x} + \frac{1}{\rho_o}\frac{\partial P'}{\partial x} - \frac{\partial}{\partial z}N\frac{\partial u}{\partial z} = 0 \tag{34}$$

$$\frac{\partial s}{\partial t} + u\frac{\partial s}{\partial x} + w\frac{\partial s}{\partial z} - \frac{\partial}{\partial z}\left(K\frac{\partial s}{\partial z}\right) = 0 \tag{35}$$

where

$$P' = \rho_o g\beta \int_z^o s\,dz'$$

is the depth-dependent internal pressure. The momentum balance at $z = -5$ m and -25 m is shown in Figure 11, and the salinity balance at the same depths is shown in Figure 12. The terms $\partial u/\partial t$, $\partial s/\partial t$ and $w\,\partial u/\partial z$ in (34) and (35) are small, and not shown in the figures. Near the head of the estuary ($x \leq 0.2\,L_l$), the momentum balance at $z = -5$ is mainly between the horizontal advection and surface pressure gradient ($u\,\partial u/\partial x \sim -1/\rho_o\,\partial P_s/\partial x$). This is expected because of strong velocity (at narrow sections) and weak salinity gradient in the area. The maximum at $x \sim 0.1\,L_l$ and the minimum at $x \sim 0.16\,L_l$ in the horizontal advective term, which correspond to the minimum and maximum in the surface pressure term, are caused by the minimum at $x \sim 0.14\,L_l$ in the width of the estuary (Fig. 13a).

Farther down in the estuary ($x \geq 0.2\,L_l$), the salinity increases significantly toward the oceanic boundary, and the velocity reduced rapidly because of the widening of the estuary. The result is that the momentum balance at $z = -5$ m is mainly between the

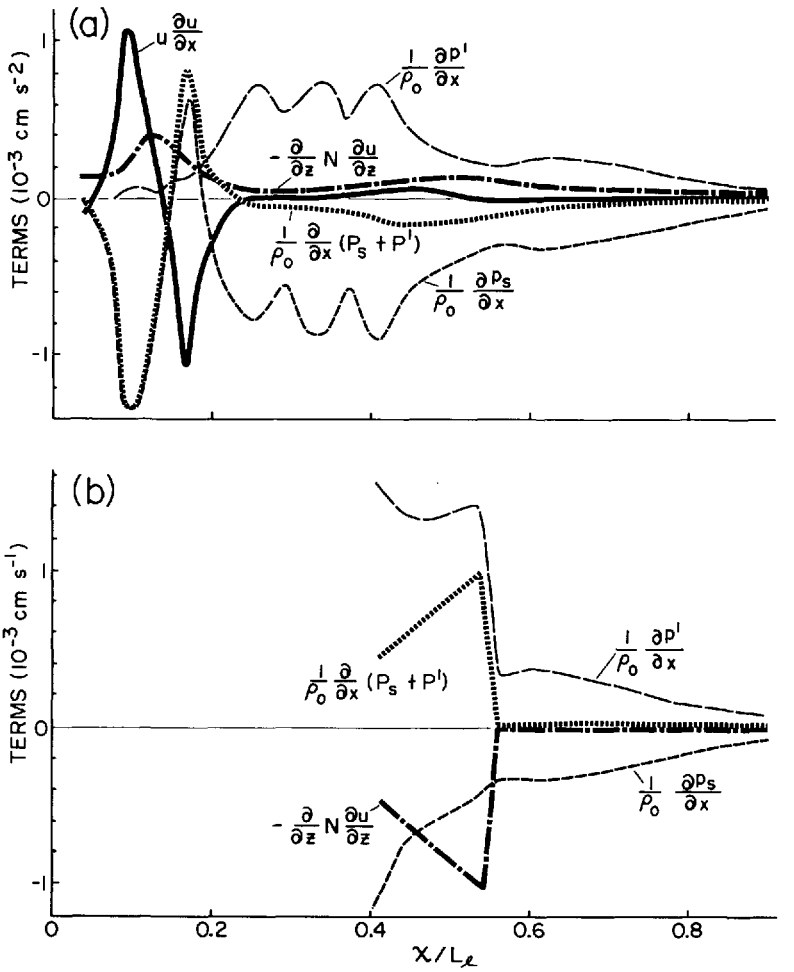

Figure 11. The balance of terms in the momentum equation (34) at day 140 (mid-May). (a) $z = -5$ m; (b) $z = -25$ m. The terms $\partial u/\partial t$ and $w\,\partial u/\partial z$ are small, and not shown in the figure.

surface pressure gradient and the pressure gradient due to the salinity variation ($\partial P_s/\partial x \sim -\partial P'/\partial x$). Because of positive salinity gradient, $\partial P'/\partial x$ is positive, and $\partial P_s/\partial x$ is negative. The vertical viscous term is positive at this depth ($z = -5$ m). The horizontal advection is insignificant at these locations except near $x \sim 0.45\ L_l$.

In the deeper water ($z = -25$ m, Fig. 11b), the momentum balance for $x \geq 0.56\ L_l$ is again mainly between $\partial P_s/\partial x$ and $\partial P'/\partial x$. However, the vertical viscous term becomes very significant for $x \leq 0.56\ L_l$. This is because strong velocity gradient is developed in the vertical column for these shallow water areas. The nonlinear advective term is small in this region. The momentum balances in deeper water ($|z| \geq 25$ m) are basically the same as those for $x \geq 0.56\ L_l$ shown in Figure 11b.

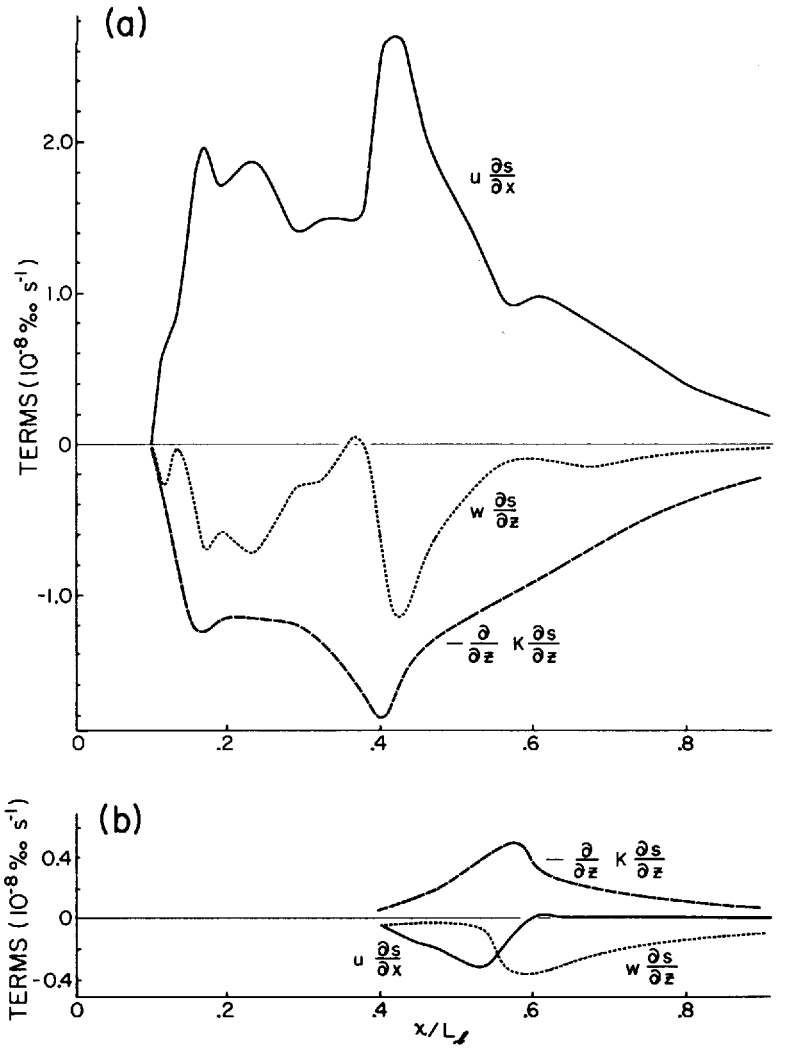

Figure 12. The balance of terms in the salinity equation (35) at day 140 (mid-May). (a) $z = -5$ m; (b) $z = -25$ m. The term $\partial s/\partial t$ is small and not shown in the figure.

By taking the depth-average of the momentum equation (34), and neglecting the accelerating and advective terms, we obtain the equation for $x \geq 0.2\ L_l$ as

$$\frac{1}{\rho_o}\frac{\partial P_s}{\partial x} = -\frac{1}{\rho_o}\frac{1}{D}\int_{-D}^{o}\frac{\partial P'}{\partial x}\,dz - \frac{\lambda u_b}{D}. \tag{36}$$

Since the effect of bottom friction on the circulation is small (Section 3b), Eq. (36) indicates that the negative mean surface pressure gradient is balanced by the positive

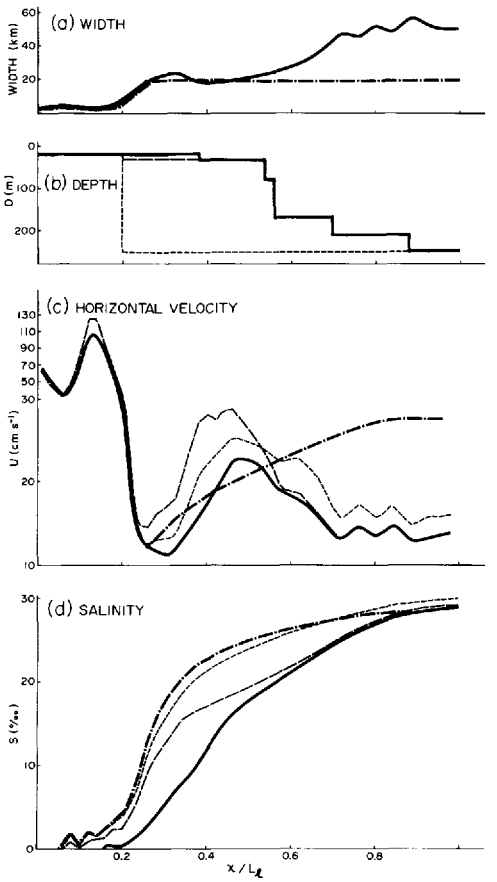

Figure 13. The studies of topographic and coastal geometrical effects on circulation and salinity in the St. Lawrence Estuary. (a) Width. Two cases are considered: (1) the width of the St. Lawrence Estuary (solid); (2) the idealized case of constant width of 20 km for $x \geq 0.26\ L_l$ (dash-dotted). (b) Depth. Three cases are considered: (1) the depth of the St. Lawrence Estuary (solid); (2) the idealized case of extending 30 m from $x = 0.38\ L_l$ to $x = 0.2\ L_l$ (long dashed); and (3) the idealized case of constant depth of 250 m for $x \geq 0.2\ L_l$ (short dashed). (c) The typical horizontal velocity (at mid-May) at $z = -5$ m. (d) The typical salinity at $z = -5$ m and at day 140 (mid-May). The curves (solid), (long dashed), (short dashed) and (dash-dotted) in (c) and (d) correspond respectively to the case of the St. Lawrence Estuary, the idealized case of extending 30 m from $x = 0.38\ L_l$ to $x = 0.2\ L_l$ [long dashed in (b)], the idealized case of constant depth of 250 m for $x \geq 0.2\ L_l$ [short dashed in (b)], and the idealized case of both constant depths of 250 m for $x \geq 0.2\ L_l$ and constant width of 20 km for $x \geq 0.26\ L_l$ [short dashed in (b) and dash-dotted in (a)].

depth-averaged internal pressure gradient induced by the positive salinity gradient. As the internal pressure gradient increases with depth, we expected that the magnitude of the surface pressure gradient is greater than that of the internal pressure gradient near the surface, and smaller in deeper water. From (34), we thus expected that the vertical viscous term is positive near the surface, and negative in deeper water (Fig. 11a, b).

In the salinity equation (35), the down-estuary advection of low salinity at $z = -5$ m is balanced by the upward advection and the diffusion of high salinity (Fig. 12a). In deeper water ($z = -25$ m, Fig. 12b), the diffusion of low salinity from upper levels is balanced by the up-estuary and upward advections of high salinity. The up-estuary advection of high salinity is small for $x \geq 0.6\ L_l$ at this depth ($z = -25$ m, Fig. 12b), and for all locations deeper than 25 m.

To examine the topographic and coastal geometrical effects on the salinity and circulation in the estuary, we perform a series of experiments using idealized depths and widths shown in Figure 13a, b. The velocity and salinity at $z = -5$ m for the experiment is shown in Figure 13c, d. By increasing the depths between $x = 0.2\ L_l$ and $x = 0.38\ L_l$ from 20 m to 30 m (long dashed in Fig. 13b), we enhance the salinity intrusion toward the head of the estuary, and thus increase the salinity and velocity at $z = -5$ m (Fig. 13c, d). As expected, the increases are more significant near the area where the depth increases. By making the depths to be a constant of 250 m for $x \geq 0.2\ L_l$ (short dashed in Fig. 13b), we further enhance the salinity intrusion which results in the larger salinity at $z = -5$ m (Fig. 13d). Although the volume transport of the estuarine circulation is also further enhanced, the velocity at $z = -5$ m between $x = 0.2\ L_l$ and $x = 0.54\ L_l$ is reduced (Fig. 13c). This is because the thickness of the upper and lower layers at these locations increase, the result of removing the limitation of layer thickness by the depth of the water column (the depths increase from 20 m or 30 m to 250 m).

By keeping the depths for $x \geq 0.2\ L_l$ to be a constant of 250 m (short dashed in Fig. 13b), but changing the width of the estuary to be a constant of 20 km for $x \geq 0.26\ L_l$ (dash-dotted in Fig. 13a), we change very significantly the velocity structure in the estuary: instead of the maximum velocity occurred at $x \sim 0.46\ L_l$ (see short dashed in Fig. 13c), the velocity increases more or less continuously from $x \sim 0.26\ L_l$ to the mouth of the estuary. This down-estuary increase of velocity is expected for the constant width case because the flow in the upper layer is intensified toward the down-estuary direction by the entrainment of the water from the lower layer. The occurrence of the maximum velocity at $z = -5$ m for $x \sim 0.45\ L_l$ for the variable width cases is the result of entrainment of the water from the lower layer, which increases the current in the down-estuary direction, and the rapid widening of the estuary for $x \geq 0.54\ L_l$, which decreases the current in the same direction. Note that the variation in the computed vertical velocity (2) between the constant and variable width cases is much smaller than that in the width of the estuary, so that the horizontal velocity can decrease with the widening of the estuary.

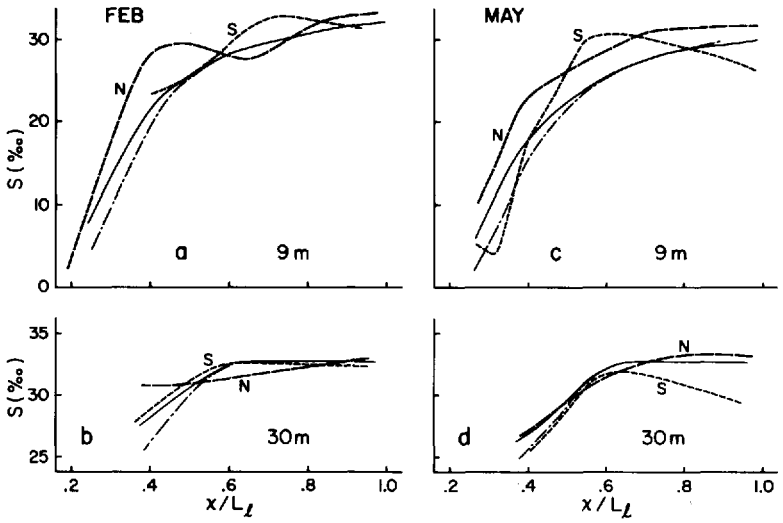

Figure 14. The comparison between the computed and observed salinity of the St. Lawrence Estuary. (a) 9 m, February; (b) 30 m, February, (c) 9 m May; and (d) 30 m, May. The observed data is taken from Neu (1970). (long dashed) The observed north shore data; (short dashed) the observed south shore data; (solid) the computed data using (Eq. 25) $a = b = 0.3 \times 10^{-3}\ m^2\ s^{-1}$; (dash-dotted) the computed data using $a = b = 0.5 \times 10^{-3}\ m^2\ s^{-1}$.

The experimental data that are used for comparison were taken by Neu in 1963 (Neu, 1970). The runoff in that year is shown in Figure 7. Two surveys were conducted in that year: one in the winter (18–25 February) and the other in the spring (21–24 May). Figure 14 shows the horizontal variation of the salinity at 9 m and 30 m. We can see that the numerical result with $a = b = 3 \times 10^{-4}\ m^2\ s^{-1}$ is generally comparable to the observation, except near the Tadoussac area ($x \approx 0.5\ L_l$) where the comparison is reasonable only for the February result. More detailed comparison cannot be performed because the experimental data (Neu, 1970) are found to be seriously contaminated by the tidal signal which has an amplitude of 1.5 to 3% in the estuary (Taylor, 1978).

5. The amplitude and arrival time of the freshwater pulse

Figure 15 shows the horizontal variation of the freshwater pulse near the surface. Toward the downstream region, we can see that the pulse generally has a smaller amplitude and arrives later. The horizontal and vertical distribution of the pulse's amplitude which is defined as the salinity difference [$\Delta s = s$(February) $- s$(minimum)] is shown in Figure 16. The maximum value of the pulse is 3.7%, and located near the surface at $x \approx 0.44\ L_l$. In the lower level ($z = 15$ m), the location of the maximum pulse moves upstream to $x \approx 0.24\ L_l$, and the amplitude reduces to 2.2%. The pulse at 5 m is larger than that at 15 m for $x \geq 0.26\ L_l$ and becomes smaller

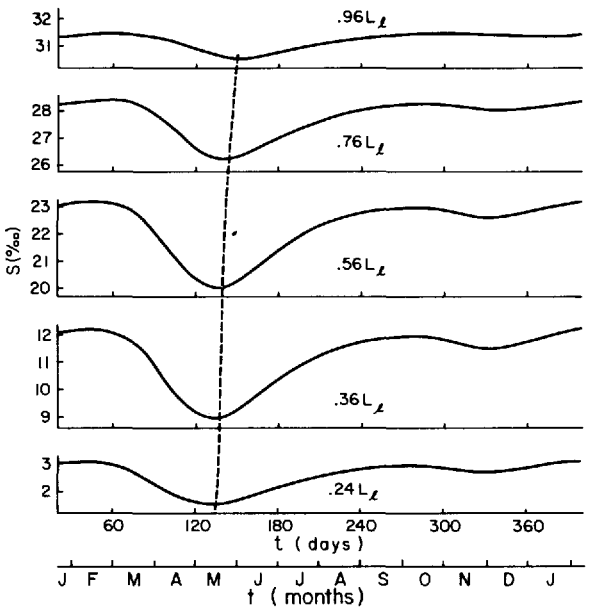

Figure 15. The horizontal variation of the freshwater pulse at 5 m of the St. Lawrence Estuary. The value on the curves indicates the distance from the head of the estuary.

upstream at those locations. At 25 m, the pulse decreases downstream from $x \approx 0.4\ L_l$, and forms a minimum around the slope region ($x \approx 0.56\ L_l$). At 35 m, the pulse becomes quite small ($\Delta s \approx 0.06\%$). In the following dynamical discussions, only the pulses at the upper three levels will be examined in detail.

The arrival time of the pulse, which is defined as the time for the occurrence of the minimum salinity is shown in Figure 17. The initial formation of the pulse occurs near

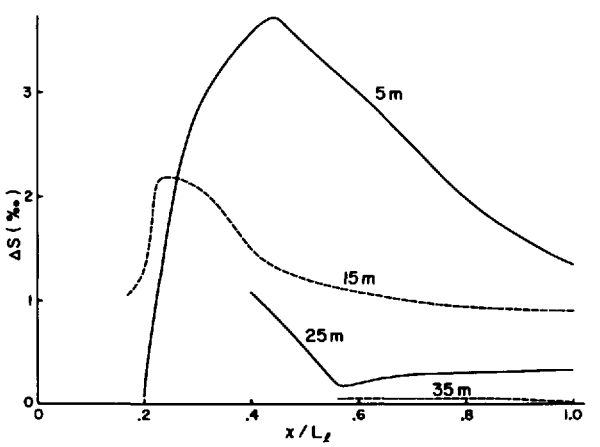

Figure 16. The amplitude of the freshwater pulse $\Delta s = s$(February) $- s$(minimum).

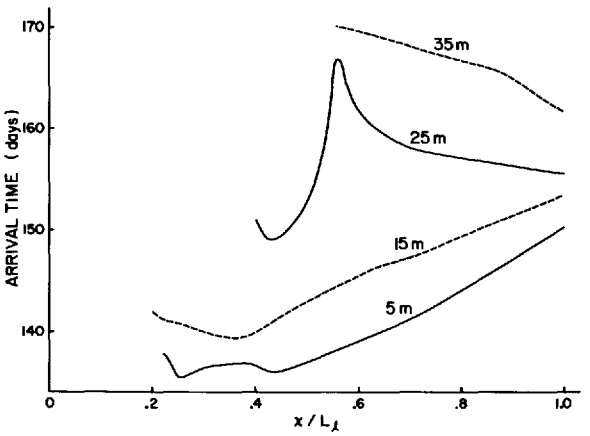

Figure 17. The arrival time of the freshwater pulse measured from the day 130 (May 10).

the surface at two locations. The first location is at $x \approx 0.25\ L_l$ which is close to the location where the amplitude of the pulse is uniform in the water column (Fig. 16). The second location is at $x \approx 44\ L_l$ which corresponds to the location of maximum pulse at 5 m. In the deeper water, the pulse arrives later. At 25 m, the arrival time has a maximum at the slope region ($x \approx 0.56\ L_l$). It is interesting to note that, in contrast to the result at the upper levels, the arrival time at or below 25 m decreases downstream from the slope region.

Observations of the freshwater pulse in the estuary and Gulf of St. Lawrence are shown in Figure 1. In the estuary, the observation includes the mean salinity data taken between 1960 to 1976 (curves A and C in Fig. 1, Neu, 1982) near Pte. aux Orignaux and Pte. des Monts (locations A and C in Fig. 2a); and the monthly averaged data along the cross-section near Rimouski during 1973 and 1974 (location B in Fig. 2, El-Sabh, 1979). The average between the surface measurement in the north and south sides of the section is shown in curve B of Figure 1. Although both the experimental and numerical data consistently indicate that the pulse exists in the estuary between May and June, detailed comparison of the observed and computed pulse is not possible because of the enormous scatter in the observed data indicated by the statistical analysis of the historical data (Dyck and LeBlond, 1981), and the weekly observations of salinity at Rimouski Harbour (El-Sabh, 1979). The exclusion of some rivers in the model, such as the Saguenay River and the Manicouagan River System, may underestimate the pulse's amplitude in the far downstream area of the estuary.

a. Salinity equation for the freshwater pulse. As the freshwater runoff changes, the governing equation for the salinity changes can be written as

$$\frac{\partial[s - s_o]}{\partial t} + \left[u\frac{\partial s}{\partial x} - u_o\frac{\partial s_o}{\partial x}\right] + \left[w\frac{\partial s}{\partial z} - w_o\frac{\partial s_o}{\partial z}\right] + \left[\frac{\partial}{\partial z}K\frac{\partial s}{\partial z} - \frac{\partial}{\partial z}K_o\frac{\partial s_o}{\partial z}\right] = 0 \quad (37)$$

where s and (u, w) are the instantaneous salinity and velocity, and s_o and (u_o, w_o) are the background values of salinity and velocity. The terms in brackets are the difference between the instantaneous and background values. For small changes of salinity (small amplitude of the pulse) computed in the St. Lawrence model, Eq. (37) can be approximated by

$$\frac{\partial s'}{\partial t} + u' \frac{\partial s_o}{\partial x} + u_o \frac{\partial s'}{\partial x} + w' \frac{\partial s_o}{\partial z} + w_o \frac{\partial s'}{\partial z} - \frac{\partial}{\partial z} K_o \frac{\partial s'}{\partial z} = 0 \tag{38}$$

where $s' = s - s_o$, $u' = u - u_o$ and $w' = w - w_o$. The equation shows that the change of the salinity (first term) is due to the change of the velocity (second and fourth terms), the advection by the background velocity (third and fifth terms), and the vertical diffusion. In the following discussions, the background salinity and velocities (s_o, u_o, w_o) are taken to be the values at day zero (the end of December).

Note that the vertical diffusion coefficient, which is found to vary less significantly than the vertical variation of salinity is approximated in (38) by its background value (K_o). By reducing the freshwater runoff, the stratification is reduced because the salinity increases more significantly toward the surface. However, the vertical velocity gradient is also reduced because the horizontal velocity generally decreases with the small runoff. Thus, the Richardson number (5), and the diffusions coefficients vary less significantly than the vertical variation of salinity.

b. The response time. To investigate the response of the system, which helps to understand the development and propagation of the freshwater pulse, we first obtain the steady state solution for R (runoff per unit width) = 5.4 $m^2 s^{-1}$ (denoted as R_1, the maximum runoff, Fig. 7), and then continue the computation by reducing the runoff to half of its value ($1/2\ R_1$) in 30 days.

By reducing freshwater runoff, the salinity of the water column is expected to increase. The salinity changes is approximated by

$$\Delta s = \delta s\ (1 - e^{-(t-t_1)/\tau}) \tag{39}$$

where $\Delta s = s - s_1$, $\delta s = s_e - s_1$, s_1 and s_e are respectively the equilibrium solutions for $R = R_1$ and $R = 1/2R_1$, and τ is the response time which indicates how fast the system approaches the equilibrium solution. The smaller the value of τ, the faster the system approaches the equilibrium state.

The response time of the St. Lawrence Estuary model is shown in Figure 18. By comparing this figure to Figure 17, we can see that the variation of the response time and the arrival time of the freshwater pulse are remarkably similar. The important correlation between these two parameters is not surprising because we expect that the faster the systems response, the sooner the pulse is formed.

The structure of the response time shown in Figure 18 is found to be insensitive to the time interval of the freshwater variation (R varies from R_1 to $1/2R_1$): the value of

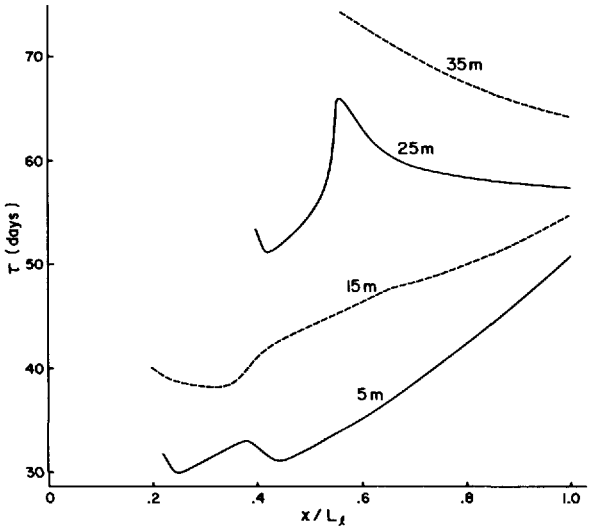

Figure 18. The response time [τ, defined in (39)] of the St. Lawrence model.

the response time increases by more or less the amount of the increase in the time interval.

c. Salinity balance near the surface ($z = -5$ m). Eq. (38) can also be written as

$$\frac{Ds'}{\partial t} + w_o \frac{\partial s'}{\partial x} + u' \frac{\partial s_o}{\partial x} + w' \frac{\partial s_o}{\partial z} - \frac{\partial}{\partial z} K_o \frac{\partial s'}{\partial z} = 0 \tag{40}$$

where $Ds'/\partial t = \partial s'/\partial t + u_o \, \partial s'/\partial x$ describes the change of the freshwater pulse at a fixed level during the advection by the background horizontal velocity. The change can be due to the advection in the vertical direction (second term), the forcings resulted from the changes in velocities (third and fourth terms), and the dissipation by the vertical diffusion (fifth term).

The difference between (40) and the governing equation for a tracer (which includes only the advection by the mean current and the dilution by vertical diffusion) is the existence of the additional terms $u'(\partial s_o/\partial x)$ and $w'(\partial s_o/\partial z)$. These additional terms describe the nonlinear interaction between the velocity and the salinity of the freshwater pulse. With the arrival of the pulse, the surface current increases ($u' > 0$), the advection of low salinity from the upstream region ($\partial s_o/\partial x > 0$) is thus increased, and the result is an increase in the amplitude of the pulse. For the forcing by the vertical advection ($w' \, \partial s_o/\partial z$), the arrival of the pulse generally increases the vertical velocity ($w' > 0$, Section 6), more saline water is thus advected toward the surface and the amplitude of the pulse is reduced. Thus, $u' \, \partial s_o/\partial x$ is generally a positive forcing for the pulse, and $w' \, \partial s_o/\partial z$ a negative forcing. Because of these nonlinear forcings, the

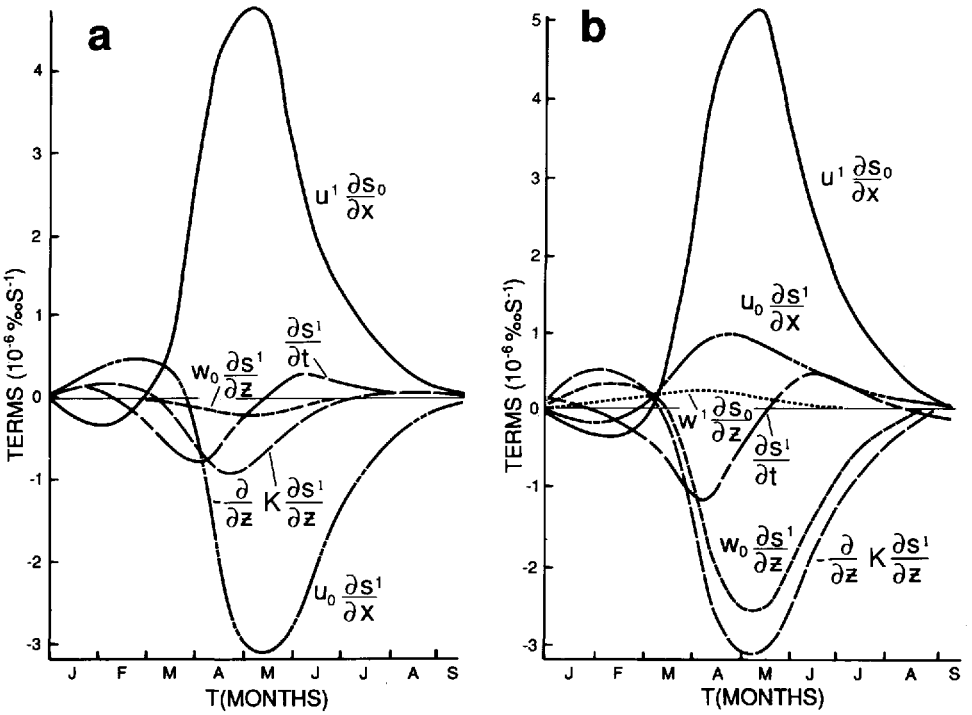

Figure 19. The balance of terms in the salinity equation (38) at $z = -5$. (a) $x = .28\ L_l$; (b) $x = .44\ L_l$.

distribution of the amplitude and arrival time of the freshwater pulse can be more complicated than that of a tracer. For example, the amplitude of the pulse can be increased in the downstream direction if the positive forcing is larger than the combination of negative forcing and dissipation. The pulse can be formed earlier in the downstream location if the strong positive forcing has a short response time.

The amplitude. An example of the salinity balance near the surface ($z = -5$ m) in the upstream region ($x \leq .4\ L_l$) is shown in Figure 19a (at $x = .28\ L_l$). In this region, the vertical advection ($w_o\ \partial s'/\partial z$) and the forcing by vertical velocity ($w'\ \partial s_o/\partial z$) are small, and the forcing by the horizontal velocity ($u'\ \partial s_o/\partial x$) is significantly larger than the dissipation. Thus, the amplitude of the pulse increases during the downstream advection (Fig. 16). Farther down in the estuary ($x > .40\ L_l$), the strong background vertical velocity (Fig. 9) significantly advects the pulse toward the surface, and thus reduces the increase of the pulse's amplitude at $z = -5$ m. The increase of the pulse's amplitude is also reduced by the stronger dissipation by vertical diffusion. An example of the salinity balance at $x = .44\ L_l$ is shown in Figure 19b. For $x > 0.44\ L_l$, the combination of vertical advection and dissipation becomes greater than the forcing by the horizontal velocity, and the pulse's amplitude becomes smaller toward the downstream direction (Fig. 16).

The arrival time. Near the head of the estuary, the salinity balance can be approximated by (Fig. 19a)

$$\frac{Ds'}{Dt} = -u'\frac{\partial s_o}{\partial x} + \frac{\partial}{\partial z}K_o\frac{\partial s'}{\partial z}. \tag{41}$$

Very close to the head of the estuary (e.g., $x \leq .24\ L_l$) where the surface velocity is found to be induced directly by the freshwater runoff through the depth-averaged velocity ($u \propto U = Q/BD$, Eq. 12). The freshwater pulse is expected to be formed quickly because the forcing by the horizontal advection ($u'\partial s_o/\partial x$) is directly proportional to the runoff. Thus, the pulse is formed initially near the head, and then advected by horizontal current toward the downstream locations.

In the St. Lawrence Estuary, the minimum arrival time of the freshwater pulse, instead of locating at the head of the estuary, occurs at $x = .25\ L_l$ and $x = 0.44\ L_l$ (Fig. 17). The reason for the occurrence at the former location ($x = .25\ L_l$) is that the formation of the pulse at the region upstream of this location is delayed by the additional forcing of vertical diffusion which transmits the low salinity signals from stronger pulse in deeper water (Fig. 16). Because of the later formation of the pulse in deeper water, it is expected that the additional forcing by the vertical diffusion has longer response time than the forcing by the horizontal advection ($u'\partial s_o/\partial x$) which has more or less the same response time as the freshwater runoff ($u' \propto Q$).

Beyond $x = .24\ L_l$, the arrival time generally increases with x except near $x = .44\ L_l$ where a small minimum is predicted (Fig. 17). The location of this minimum coincides with that of the maximum amplitude of the pulse (Fig. 16). The dynamics associated with the occurrence of this second minimum, which involve complex salinity balances between horizontal and vertical advections, and vertical diffusion, are not clear.

A tracer. As shown in Figures 17 and 18, the response time and the arrival time of the freshwater pulse near the surface increases toward the ocean from the location of the minimum response time (at $x = .44\ L_l$). This increase is due to the advection of the salinity signal from the location of the maximum s'. If we regard the freshwater pulse as a tracer, the arrival time (T) of the freshwater pulse at the downstream location can be estimated as

$$T \approx T_o + X_a/\overline{u}$$

where T_o is the time required for the first formation of the freshwater pulse, X_a the distance from the location of maximum s', and $\overline{u}$ the average horizontal velocity over the distance X_a. The time taken by the freshwater pulse to arrive at the oceanic boundary from its formation at $X \approx 0.44\ L_l$ is $\approx$ 18 days ($X_a \approx 2.66 \times 10^5$ m and $\overline{u} \approx 0.17$ m s^{-1}), which is comparable to the computed value of 14 days (Fig. 17). The value is also comparable to 20 days, the difference between the response time at the oceanic boundary and at the location of minimum response time ($x \approx 0.44\ L_l$, Fig. 18).

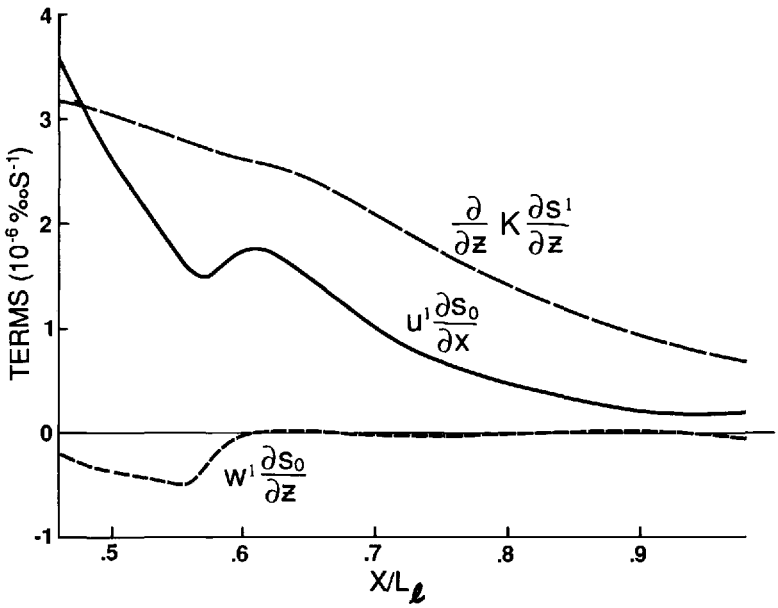

Figure 20. The comparison of the vertical diffusion $[\partial/\partial z(K_o\, \partial s'/\partial z)]$ and the vertical advection $[u'\, \partial s_o/\partial x,\ w'\partial s_o/\partial z]$ at day 140 (mid-May).

By regarding the freshwater pulse as a tracer, although the arrival time can be estimated reasonably well, the pulse's amplitude cannot be predicted accurately. This is because the pulse involves nonlinear interaction between velocity and salinity. For a tracer, the downstream reduction of the amplitude near the surface is caused by the vertical diffusion. For the freshwater pulse, because the horizontal velocity induced by the pulse produces strong positive forcing of $u'\, \partial s_o/\partial x$, the downstream reduction of the pulse's amplitude is significantly less than that of a tracer.

Figure 20 shows the horizontal variation of the forcings, $u'\ (\partial s_o/\partial x)$ and $w'(\partial s_o/\partial x)$, and the vertical diffusion on day 140 (mid-May, which is approximately the time for the pulse to occur in the estuary). In comparison with the vertical diffusion, the total forcing, $u'(\partial s_o/\partial x) + w'(\partial s_o/\partial x)$, is about the same near the location of the maximum amplitude ($x = .44\ L_l$) and decreases to about $\frac{1}{3}$ at the mouth of the estuary ($x = L_l$). The average ratio of total forcing to vertical diffusion is 0.46. Thus, the amplitude of the freshwater pulse will be reduced much faster (about 1.5 times) during the downstream advection if the pulse is regarded as a tracer.

d. Salinity balance at the second level ($z = -15$ m). As the freshwater runoff increases, the estuarine circulation is expected to increase, resulting in the increase of the vertical velocity in most of the area ($w' > 0$, see Section 6). However, near the head of the estuary, the increase of the freshwater runoff pushes the salinity intrusion away

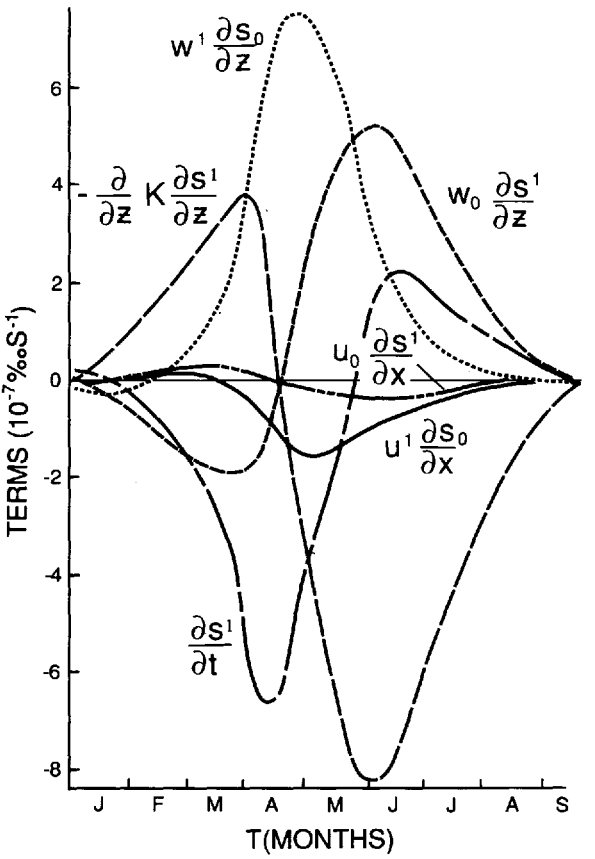

Figure 21. The balance of terms in the salinity equation (38) at $z = -15$ m and $x = .24\ L_I$.

from the head, and reduces the two-layer circulation. The vertical velocity is thus reduced near the head of the estuary ($w' < 0$). Since the induced downwelling ($w' < 0$) advects low salinity from surface to deeper water, it produces a positive forcing ($w' \partial s_o/\partial z$) for the freshwater pulse in the lower layer. An example of the salinity balance near the head of the estuary at $z = -15$ m is shown in Figure 21 (at $x = .24\ L_I$). During the initial period of higher runoff, the combination of vertical diffusion and downward advection ($w'\partial s_o/\partial x$) of low salinity water quickly decreases the salinity in the lower layer (Fig. 21). However, as the salinity decrease ($s' < 0$) in the lower layer becomes more significant than that in the upper layer (after mid-April) more saline water is diffused to the lower layers, and thus slows down the decrease of the salinity in these layers. Physically, it is not surprising that, near the head of the estuary, the pulse in lower layers can be larger than that in the upper layer (for $x \leq .26\ L_I$, Fig. 16). This is because the background salinity near the surface there is near zero, and is not expected to reduce significantly for higher runoff (salinity cannot be reduced below zero). On

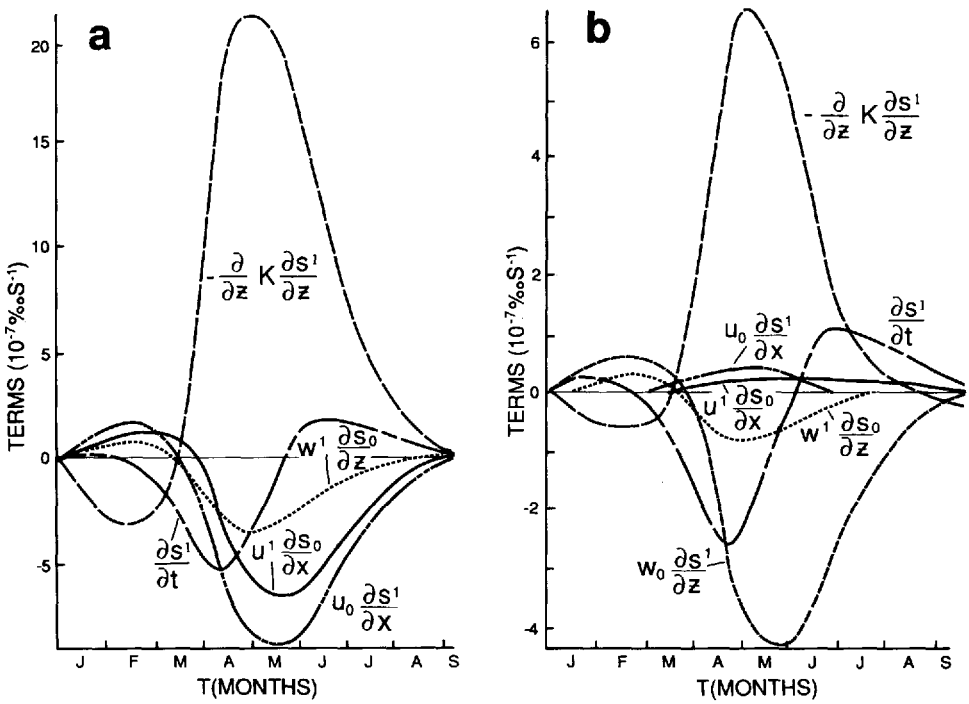

Figure 22. The balance of terms in the salinity equation (38) at $z = -15$ m. (a) $x = .36\ L_l$; (b) $x = .80\ L_l$.

the other hand, the salinity in the lower layer, which can be significantly different from zero at the same horizontal location because of the salinity intrusion from the ocean to the estuary, can be greatly reduced because the salinity intrusion is pushed toward the ocean by higher runoff.

Near the region where the salinity intrusion ends, the salinity is near zero, and the salinity pulse in the lower layer is expected to be small. Thus, the pulse is reduced toward the head of the estuary for $x \leq .24\ L_l$.

Beyond $x = .24\ L_l$, the salinity balance at $z = -15$ m can be divided into two regions. In the deep water region of $x \geq .4\ L_l$ (depth ≥ 30 m), the vertical diffusion of low salinity ($\partial/\partial z\ K_0\ \partial s'/\partial z$) is mainly balanced by the upward vertical advection by background vertical velocity ($w_o\ \partial s'/\partial z$). An example is shown in Figure 22b for $x = .8\ L_l$. The horizontal advections ($u_o\ \partial s'/\partial x$, $u' \partial s_o/\partial x$) are small here. The reason for the downstream decrease of the pulse's amplitude is that the surface pulse is smaller and diffuses smaller signal to the deeper water. The increase of the arrival time toward the oceanic boundary follows that of the surface pulse.

In the shallow water region of $.24\ L_l < x < .4\ L_l$, (depth = 20 m), the upstream advection at $z = -15$ m becomes significant. Figure 22a shows the salinity balance at $x = .36\ L_l$. The advections by induced velocities ($u' \partial s_o/\partial x$, $w' \partial s_o/\partial z$) produce negative

forcings to the pulse because the increase of vertical velocity and upstream velocity by higher runoff (stronger estuarine circulation) advects smaller signals of the freshwater pulse from deep water and downstream regions. As the pulse is advected by the background currents (u_o) toward the head of the estuary, the amplitude of the pulse increases (Fig. 16) because the positive forcing by the vertical diffusion of the surface pulse is larger than the negative forcings by the horizontal and vertical advections. The upstream advection of the pulse by the background velocity ($u_o\, \partial s_i/\partial x$) indicates that the arrival time increases toward the head of the estuary (for $x < .34\ L_l$, Fig. 17, 18).

e. Salinity balance at the third level ($z = -25$ m). Upstream of $x = .56\ L_l$, the amplitude of the pulse at $z = -25$ m increases rapidly. This is because, as the pulse is advected toward the head of the estuary, the amplitude of the pulse is increased by the positive forcing of diffusion of the pulse from upper levels which is larger than the negative forcings of the horizontal and vertical advections.

Beyond $x = .56\ L_l$, the amplitude of the pulse at $z = -25$ m also increases toward the oceanic boundary (Fig. 16), which does not correspond to the downstream decrease of the pulse in the upper levels, and of the forcing by the vertical diffusion. The cause for the increase is the spatial variation of the vertical velocity. Because the upwelling is much stronger near the slope region than in the downstream locations, the negative (upward) forcing by the background vertical current ($w_o\, \partial s'/\partial z$) reduces more significantly the amplitude of the pulse near the slope region. Figure 23 compares the salinity balance near the slope region (at $x = .6\ L_l$, Fig. 23a), and that near the mouth of the estuary (at $x = .8\ L_l$, Fig. 23b). We can see that, although the magnitudes of the vertical diffusion and the negative forcing by the induced vertical velocity ($w'\partial s_o/\partial z$) at $x = .6\ L_l$ is about twice of those at $x = .8\ L_l$, the magnitude of the negative forcing by the background vertical velocity ($w_o\partial s'/\partial z$) at the upstream location is about three times of that at the downstream location.

The strong upwelling of the pulse by the background current near the slope region indicates that the pulse there is originated from a deep water region of the lower estuary through the horizontal (upstream) and vertical (upward) advections. Because the pulse's arrival time is large in the deep water region, it is expected that the arrival time is also large near the slope region (Fig. 17).

Upstream of the slope region, although the pulse is advected upstream by the background current, u_o, the arrival time is found to decrease toward the head of the estuary (Fig. 17). This is because the formation of the pulse is affected more strongly by the vertical diffusion than by the horizontal advection. In the upstream region, because the surface pulse arrives earlier, the vertical diffusion of the surface pulse tends to shorten the pulse's formation time. Upstream of the slope region, the positive forcing of vertical diffusion at $z = -25$ m is very strong, indicated by the rapid increase of the pulse's amplitude toward the head of the estuary (Fig. 16). Thus, although the effect of the upstream horizontal advection tends to delay the formation of the pulse in

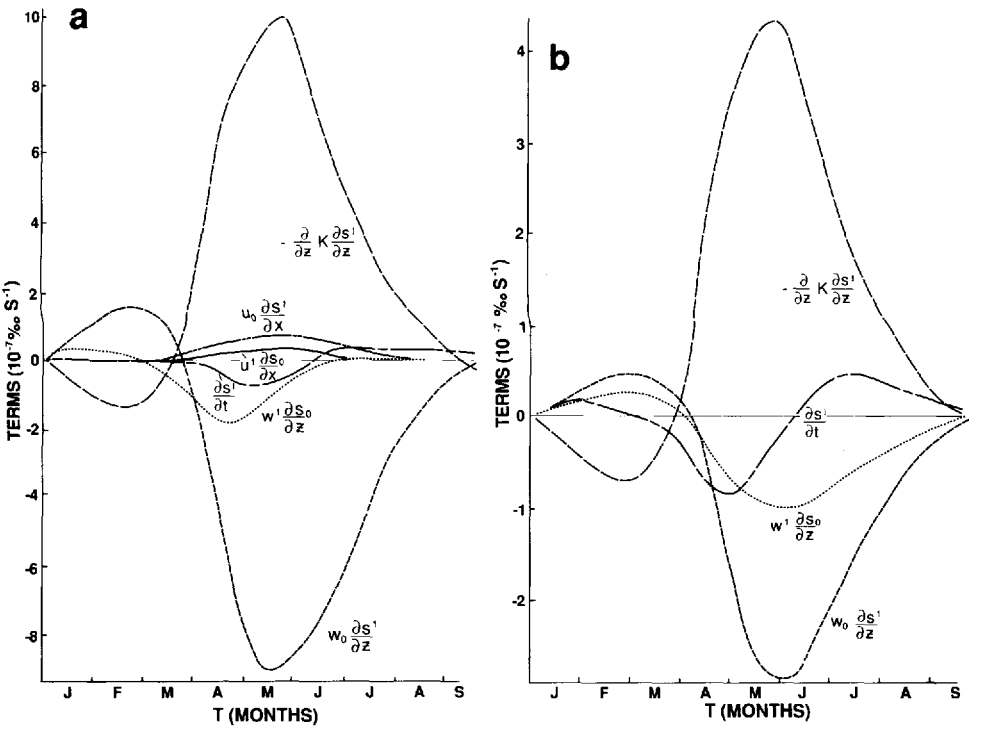

Figure 23. The balance of terms in the salinity equation (38) at $z = -25$ m. (a) $x = .60\ L_l$; (b) $x = .80\ L_l$.

the upstream region, the stronger effect of the vertical diffusion contributes to the earlier formation of the pulse (or minimum salinity) in this region.

6. The velocity response to the freshwater pulse

The time variation of the horizontal velocity at $x \approx 0.76\ L_l$ is shown in Figure 24. We can see that, with the arrival of the pulse, the velocity increases near the surface ($z \leq 15$ m) and decreases in the deep water ($z \geq 45$ m). In the intermediate water, the velocity decreases initially as the pulse arrives, and then increases later. The change of the velocity is most significant near the surface.

The minimum salinity is found to lag the maximum velocity in the lower portion of the estuary (deep water region). For the velocity shown in Figure 24 (at $x = .76\ L_l$), the phase lag is about 20 days (Fig. 25a). However, in the upper portion of the estuary (shallow water region), the occurrence of the maximum surface velocity corresponds closely to that of the minimum salinity. An example of the salinity and velocity variation at $x = .36\ L_l$ is shown in Figure 25b.

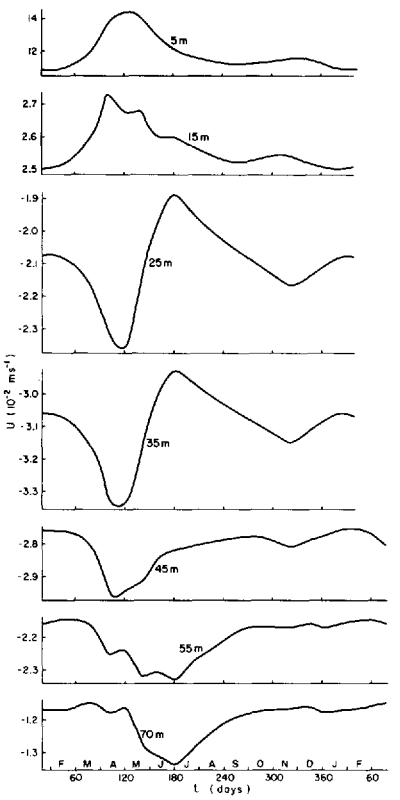

Figure 24. The seasonal variation of the horizontal velocity u at $x = .76\ L_I$.

In the lower portion of the estuary where the nonlinear advective terms are small, the momentum equation can be reduced from (34) to

$$\frac{\partial}{\partial z} N_o \frac{\partial u'}{\partial z} = g\beta \int_{z^*}^{o} \frac{\partial s'}{\partial x} dz + \frac{1}{\rho_o} \frac{\partial P_s'}{\partial x} \tag{42}$$

where $P_s' = P_s - P_{so}$ and P_{so} is the background surface pressure. Taking the depth-average of (42), using the boundary condition of zero surface stress ($\partial u'/\partial z = 0$), and neglecting the small bottom stress, the surface pressure gradient can be computed from

$$\frac{1}{\rho_o} \frac{\partial P_s'}{\partial x} \approx -\frac{1}{D} g\beta \int_{-D}^{o} \int_{z^*}^{o} \frac{\partial s'}{\partial x} dz\, dz^*. \tag{43}$$

Since the pulse is concentrated near the surface (Fig. 16), we can expect from (42) and (43) that u' varies with $\partial s'/\partial x$ near the surface. An example of the time variation of

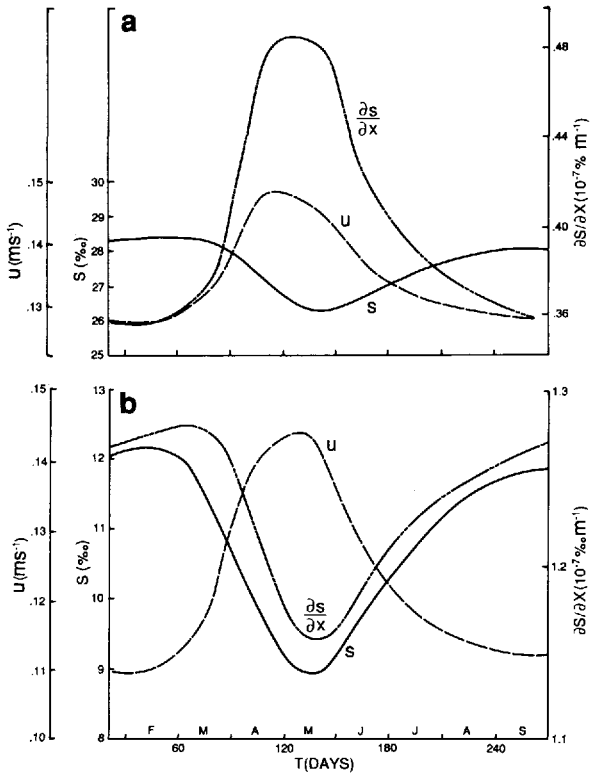

Figure 25. The seasonal variation of the velocity u, the salinity s and the salinity gradient $\partial s/\partial x$ at $z = -5$ m. (a) $x = .76\ L_l$; (b) $x = .36\ L_l$.

$\partial s/\partial x$ is shown in Figure 25. We can see that the maximum u (or u') and $\partial s/\partial x$ (or $\partial s'/\partial x$) occur more or less at the same time.

To examine the phase difference between s and $\partial s/\partial x$ (or u), we approximate the freshwater pulse as

$$s = s_o - s^* \cos \sigma\left(t - \frac{x}{\overline{u}}\right) \tag{44}$$

where s_o is the background salinity, s^* the amplitude of the pulse, σ the frequency (seasonal cycle), and $\overline{u}$ the mean downstream velocity. From (44), $\partial s/\partial x$ can be computed from

$$\frac{\partial s}{\partial x} = \frac{\partial s_o}{\partial x} + \frac{s^*\sigma}{\overline{u}} \cos\left[\sigma\left(t - \frac{x}{\overline{u}}\right) + 90°\right] - \frac{\partial s^*}{\partial x} \cos \sigma\left(t - \frac{x}{\overline{u}}\right). \tag{45}$$

The second term on the right-hand side of (45), arisen from the downstream advection of freshwater pulse, has 90° phase lead over the minimum salinity. Thus, the earlier

formation of maximum $\partial s/\partial x$ (or u) over minimum salinity in the lower portion of the estuary (Fig. 25a) is due to the downstream increase of the pulse's arrival time (Figs. 17, 18).

In the upstream shallow water region of the estuary, the nonlinear advective term becomes significant. Near the surface, the momentum balance of the velocity induced by the freshwater pulse (u') can be approximated from (34) as

$$\left[\frac{1}{2}\frac{\partial}{\partial x}(u^2 - u_o^2)\right] - \frac{\partial}{\partial z}N_o\frac{\partial u'}{\partial z} = -g\beta\int_z^o \frac{\partial s'}{\partial x}\,dz - \frac{1}{\rho_o}\frac{\partial P'}{\partial x}. \tag{46}$$

The advective term is negligible in deeper water. By taking the depth-average of (46), and again neglecting the bottom stress, we obtain

$$\frac{1}{\rho_o}\frac{\partial P_s'}{\partial x} \approx -\frac{1}{D}g\beta\int_{-D}^o\int_z^o \frac{\partial s'}{\partial x}\,dz'\,dz - \frac{\Delta z_1}{D}\left[\frac{1}{2}\frac{\partial}{\partial x}(u^2 - u_o^2)\right] \tag{47}$$

where Δz_1 is the thickness of the first level. Substitute $\rho_o^{-1}\,\partial P_s'/\partial x$ from (47) to (46), the momentum equation can be written as

$$\left[1 - \frac{\Delta z_1}{D}\right]\left[\frac{1}{2}\frac{\partial}{\partial x}(u^2 - u_o^2)\right] - \frac{\partial}{\partial z}N_o\frac{\partial u'}{\partial z} = -g\beta\left[\int_z^o \frac{\partial s'}{\partial z}\,dz' - \frac{1}{D}\int_{-D}^o\int_z^o \frac{\partial s'}{\partial x}\,dz'\,dz\right]. \tag{48}$$

If the momentum balance in (48) is between the vertical diffusion and pressure gradient, u is also expected to vary with $\partial s/\partial x$. However, because the pulse's arrival time in this region varies less significantly than that in the deep water region (Fig. 17), the maximum u and $|\partial s/\partial x|$ ($\partial s'/\partial x$ is negative for $x < .44\ L_l$) are expected to occur more closely with the minimum s in the shallow water region.

If the momentum balance in (48) is between the nonlinear advective term and the pressure term, the maximum velocity will occur more or less simultaneously with the minimum salinity. Thus, both the nonlinear advection and vertical diffusion produce the effects that the lag between maximum velocity and minimum salinity in the shallow region is smaller than that in the deep water region (Fig. 25).

In the far upstream region ($x < .3\ L_l$), the salinity balance near the surface is mainly bewteen $u'\partial s_o/\partial x$ and $u_o\,\partial s_1/\partial x$ (Fig. 19a). Thus, u varies with $\partial s/\partial x$. Again, because the pulse's arrival time in this region varies less significantly than that in the deep water region, the lag between the maximum velocity and minimum salinity in this region is smaller.

Except near the head of the estuary ($x < .26\ L_l$), the vertical velocity increases with the arrival of the pulse (Fig. 26). With the increase of the freshwater runoff, the two-layer estuarine circulation is intensified, resulted in the increase of the upwelling in the water column.

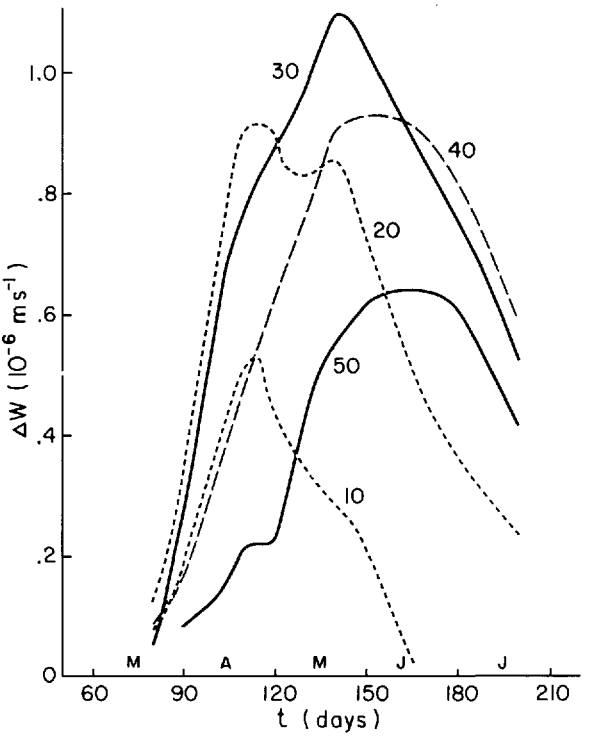

Figure 26. The time variation of the vertical velocity relative to the day 20[$\Delta w = w - w(20)$] at $x = 0.76\ L_l$. The number on the curves indicates the corresponding depths.

7. Summary and conclusions

A two-dimensional numerical model with application to the St. Lawrence Estuary was developed to investigate the freshwater pulse (characterized by a minimum salinity) in the St. Lawrence Estuary. The stratification effect on the vertical eddy coefficients increases the salinity and estuarine circulation in the upper portion of the estuary (shallow water) and decreases that in the lower portion of the estuary (mostly deep water). When freshwater runoff is doubled, the salinity decreases and the velocity increases. Instead of the two-layer flow observed for small runoff in shallow estuaries, a small outflow can be induced in the deep water for large runoff, and it splits the inflow near the slope region creating a second maximum outflow near the mouth of the estuary.

The freshwater pulse in the St. Lawrence Estuary was simulated using the seasonal variation in the freshwater runoff. The amplitude and the arrival time of the pulse are shown in Figures 16 and 17. In addition to simulating the downstream propagation and the reduction of the pulse's amplitude toward both the ocean and the deep water in most of the area, several interesting results were produced. These include the finding of

the maximum and minimum amplitudes of the pulse, the increase of the amplitude from surface to deep water for $x \leq 0.26\ L_l$, the early formation of the pulse at two surface locations ($x \approx 0.25, 0.44\ L_l$), the increase of the arrival time from surface to deep water, and the increase of the arrival time for deep water pulses (at 25 m or deeper) toward the slope region.

The velocity response to the pulse is shown in Figures 24 and 26. With the arrival of the pulse, the current increases near the surface, and decreases in the deep water. In the intermediate water, the current decreases initially as the pulse arrives, and increases later. Near the surface, the pulse lags the maximum velocity in the lower portion of the estuary (deep channel), and occurs simultaneously with the maximum velocity in the upper portion (shallow channel). For the vertical velocity, an additional upwelling is induced by the pulse.

Dynamics associated with the distribution, formation and propagation of the pulse, which are interesting and complicated are discussed in detail.

Acknowledgment. The authors thank a reviewer of the journal for many useful suggestions.

REFERENCES

Blumberg, A. F. 1975. A numerical investigation into the dynamics of estuarine circulation. Technical Report 91, Reference 75–9, Chesapeake Bay Institute, the Johns Hopkins University, Baltimore, MD, 110 pp.

Borne de Grandpre, C. de and M. I. El-Sabh. 1980. Etude de la circulation verticale dans l'estuaire du Saint-Laurent au moyen de la modelisation mathematique. Atmos.-Ocean, *18,* 304–321.

Borne de Grandpre, C. de, M. I. El-Sabh and J. C. Solomon. 1981. A two-dimensional numerical model of the vertical circulation of tides in the St. Lawrence Estuary. Estuar. Coastal Mar. Sci., *12,* 375–387.

Bowden, K. R. and P. Hamilton. 1975. Some experiments with a numerical model of circulation and mixing in a tidal estuary. Estuar. Coastal Mar. Sci., *3,* 281–301.

Bryan, K. 1969. A numerical method for the study of the circulation of the world ocean. J. Computat. Phys., *4,* 347–376.

Dyck, K. and P. H. LeBlond. 1981. Saint Lawrence Estuary Runoff-Salinity Correlations, Univ. British Columbia (Vancouver, Canada) Manuscript Report No. 37, 105 pp.

El-Sabh, M. I. 1973. Seasonal and long term variations of the water properties in the Gulf of St. Lawrence, *in* Proc. Workshop on the Physical Science in the Gulf and Estuary of St. Lawrence, M. I. El-Sabh, ed., Univ. Quebec Rimouski, Quebec, 128–158.

—— 1977. Circulation pattern and water characteristics in the lower St. Lawrence Estuary, *in* Proc. of Symposium on Modelling Transport Mechanisms in Oceans and Lakes, T. S. Murty, ed., Environment Can. Report No. 43, 243–248.

—— 1979. The lower St. Lawrence Estuary as a physical oceanography system. Naturaliste Can., *106,* 55–73.

El-Sabh, M. I., H. J. Lie and V. G. Koutitonsky. 1982. Variability of the near-surface residual current in the lower St. Lawrence Estuary. J. Geophys. Res., *87,* 9589–9600.

Festa, J. F. and D. V. Hansen. 1976. A two-dimensional numerical model of estuarine

circulation: the effects of altering depth and river discharge. Estuar. Coastal Mar. Sci., *4,* 309–323.

Forrester, W. D. 1967. Current and geostrophic currents in the St. Lawrence Estuary. Bedford Institute of Oceanography Report *67–5,* 175 pp.

Hamilton, P. 1975. A numerical model of the vertical circulation of tidal estuaries and its application to the Rottordam Waterway. Geophys. J. R. Astr. Soc., *40,* 1–21.

Hess, K. W. 1976. A three-dimensional numerical model of the estuary circulation and salinity in Narragansett Bay. Estuar. Coastal Mar. Sci., *4,* 325–338.

Jordan, F. 1973. The St. Lawrence system runoff estimates (1960–1970). Bedford Institute of Oceanography Data Series, BI-D-73-10, 11 pp.

Lauzier, L. 1957. Variations of temperature and salinity in shallow water of the southwestern Gulf of St. Lawrence. Bull. Fish. Res. Board Can., *111,* 251–268.

Leendertse, J. J. and S. K. Liu. 1975. Modelling of three-dimensional flows in estuaries, P-5461, The Rand Corporation Publication, 18 pp.

Neu, H. J. A. 1970. A study of mixing and circulation in the St. Lawrence Estuary up to 1964. Bedford Institute of Oceanography, AOL Report 1970-9, Darthmouth, N.S., 31 pp, (Unpublished Manuscript).

—— 1982. Man-made storage of water resources—a liability to the ocean environment? Part I, Mar. Pollution Bull., *13,* 7–12.

Orlanski, J. 1976. A simple boundary condition for unbounded hyperbolic flows. J. Computat. Phys., *21,* 251–269.

Pritchard, D. W. 1954. A study of the salt balance in a costal plain estuary. J. Mar. Res., *13,* 133–144.

—— 1956. The dynamic structure of a coastal plain estuary. J. Mar. Res., *15,* 33–42.

Semtner, A. J. 1974. An oceanic general circulation model with bottom topography, Tech. Rep. *9,* University of California. 99 pp.

Taylor, G. B. 1978. Oceanographic Observations in the River, Estuary and Gulf of St. Lawrence, 30 March–26 April 1974. Bedford Institute of Oceanography Data Series/ BI-D-78-1, 76 pp.

Wang, D. P. and D. W. Kravitz. 1980. A semi-implicit two-dimensional model of estuarine circulation. J. Phys. Oceanogr., *10,* 441–454.

Received: *18 September, 1985;* revised: *9 June, 1987.*